Low energy properties of the Kondo chain in the RKKY regime

2016 New J. Phys. 18 053004

(http://iopscience.iop.org/1367-2630/18/5/053004)

New Journal of Physics
The open access journal at the forefront of physics

Deutsche Physikalische Gesellschaft DPG
IOP Institute of Physics

Published in partnership with: Deutsche Physikalische Gesellschaft and the Institute of Physics

OPEN ACCESS

RECEIVED
23 December 2015

REVISED
4 March 2016

ACCEPTED FOR PUBLICATION
5 April 2016

PUBLISHED
3 May 2016

PAPER

Low energy properties of the Kondo chain in the RKKY regime

D H Schimmel[1], **A M Tsvelik**[2,4] **and O M Yevtushenko**[1,3]

[1] Ludwig Maximilians University, Arnold Sommerfeld Center and Center for Nano-Science, Munich, D-80333, Germany
[2] Condensed Matter Physics and Material Sciences Division, Brookhaven National Laboratory, Upton, NY 11973-5000, USA
[3] Institute for Theoretical Physics, Universität Erlangen-Nürnberg, Staudtstrasse 7, D-91058 Erlangen, Germany
[4] Author to whom any correspondence should be addressed.

E-mail: tsvelik@gmail.com

Keywords: helical symmetry, ideal protected transport, Kondo chain, RKKY

Abstract

We study the Kondo chain in the regime of high spin concentration where the low energy physics is dominated by the Ruderman–Kittel–Kasuya–Yosida interaction. As has been recently shown (Tsvelik and Yevtushenko 2015 *Phys. Rev. Lett.* **115** 216402), this model has two phases with drastically different transport properties depending on the anisotropy of the exchange interaction. In particular, the helical symmetry of the fermions is spontaneously broken when the anisotropy is of the easy plane type. This leads to a parametrical suppression of the localization effects. In the present paper we substantially extend the previous theory, in particular, by analyzing a competition of forward- and backward- scattering, including into the theory short range electron interactions and calculating spin correlation functions. We discuss applicability of our theory and possible experiments which could support the theoretical findings.

1. Introduction

The Kondo chain (KC) is one of the archetypal models for interacting low-dimensional systems which has been intensively studied during the past two decades [1–11]. It consists of band electrons on a one-dimensional lattice which interact with localized magnetic moments; electron–electron interactions can also be included in the consideration [1, 2, 5, 9, 12]. The KC is not exactly solvable, nevertheless, a lot is known about it both from numerical and analytical studies [1, 6–9]. In particular, ground state properties are known from DMRG for the isotropic point [13].

One possible realization of KC is a cleaved edge overgrowth GaAs quantum wire doped with magnetic ions. Such quantum wires were manufactured a long time ago [14, 15] and have been successfully used to study one-dimensional strongly correlated physics (see, for example, [16, 17]). Functionalizing them with dynamical magnetic impurities could yield an experimental realization of the KC. As another possible platform for KC one may use carbon nanotubes functionalized with magnetic ions or molecules containing magnetic ions (possible realizations can be found in [18–20]). Alternatively one may search for quasi one-dimensional structures with coexisting localized and delocalized electrons in bulk materials. The theory predicts that in iron-based ladder materials some of the iron d-orbitals are localized and some are itinerant [21–23]. The issue is to find such crystal structures where the ladders would be sufficiently isolated from each other to prevent three-dimensional ordering (three-dimensional ordering seems to occur in $BaFe_2Se_3$ [24]).

It has been recently shown by two of us that the KC may display a rather nontrivial physics in the anisotropic regime away from half-filling in the case of dense spins when the Ruderman–Kittel–Kasuya–Yosida (RKKY) exchange interaction dominates the Kondo screening [25]. We considered an anisotropic exchange interaction with the anisotropy of the XXZ-type. Then there are two phases with different low-energy properties, namely, the easy axis (EA) phase and the easy plane (EP) one. In the EA phase, all single fermion excitations are gapped. The charge transport is carried by collective excitations which can be easily pinned by ever present potential disorder. The situation is drastically different in the EP phase. The minimum of the ground state energy corresponds to the helical spin configuration with wave vector $2k_F$ (k_F being the Fermi wave vector) which opens a gap in the spectrum of the

fermions of a particular helicity while the electrons having the other (opposite) helicity remain gapless. We remind the readers that the helicity is defined as $\mathrm{sgn}(v)\,\mathrm{sgn}(\sigma)$, where v and σ the the electron velocity and its spin, respectively. This corresponds to the spontaneous breaking of the discreet $\mathbb{Z}_2$ helical symmetry. If the potential disorder is added to the phase with the broken symmetry a single-particle backscattering is prohibited either by spin conservation (for electrons with the same helicity) or by the gap in one of the helical sectors (for electrons with different helicity). This is similar to the absence of the single-particle back-scattering of edge modes in time-reversal invariant topological insulators [5, 26–32] and results in suppression of localization effects. The latter can appear only due to collective effects resulting in a parametrically large localization radius. In other words, ballistic charge transport in the EP phase has a partial symmetry protection which is removed either in very long samples or if the spin $U(1)$ symmetry is broken. This is also similar to the symmetry protection of the edge transport in 2d topological insulators: transport is ideal if time-reversal symmetry and spin $U(1)$ symmetry are present. However, it can be suppressed in a long sample due to spontaneously broken time-reversal symmetry [33, 34].

In the present paper, we continue to study the KC in the RKKY regime where the low energy physics is governed by the fermionic gaps. We aim to explain in more details the results of [25] and to substantially extend the theory, in particular, by analyzing the role of forward scattering (i.e., of the Kondo physics), by taking into account the short range electron interactions and by calculating the spin correlation functions.

Similar ideas to those presented here were already pursued in [2], where the emergence of helical order was recognized. In contrast to [2] we take into account the dynamics of the lattice spins whose presence substantially modifies the low-energy theory.

The Hamiltonian of the KC on a lattice is

$$\mathcal{H} = \mathcal{H}_0 + \mathcal{H}_{\mathrm{int}} = \sum_i [t c^\dagger_{i+1} c_i + \mathrm{h.c.}] + \sum_a \sum_{j\in M} J^a S^a_j c^\dagger_j \sigma^a c_j,\ a = x, y, z; \tag{1}$$

where t is the hopping matrix element, $c_i^{(\dagger)}$ annihilates (creates) an electron at site i, $\boldsymbol{S}_i$ is a local spin of magnitude s, σ^a is a Pauli matrix, and M constitutes a subset of all lattice sites. J denotes the interaction strength between the impurities and the electrons. We distinguish J_z and $J_x = J_y =: J_\perp$. Short range interactions between the electrons will be added later in section 4.4. The dynamics of a chain of spins will be added in section 2. We will be interested in the case of dense magnetic impurities, $\rho_s\,\xi_0 \gg 1/L_K$ (with the impurity density ρ_s and the single-impurity Kondo length L_K), when the effects of the electron-induced exchange can take predominance over the Kondo screening. The paper is organized as follows: we first introduce a convenient representation of the impurity spins in section 2. Necessary conditions for the RKKY regime are then discussed in section 3. The gap is studied in section 4. In section 5 we compute the conductance and analyze the effects of spinless disorder. The spin-spin correlation functions are given in section 6.

2. Formulation of the low energy theory

To develop a low energy description of the KC model (1) we have to single out slow modes and integrate over the fast ones. As the first step, we need to find a convenient representation of the spins such that it will be easy to separate the low and high energy degrees of freedom.

2.1. Separation of scales in the spin sector

Consider first a single spin. It is described by the Wess–Zumino term in the action [35]

$$S_{\mathrm{WZ}} = \mathrm{i}\int_0^1 \mathrm{d}u \int_0^\beta \mathrm{d}\tau \frac{s}{8\pi}\epsilon^{\mu\nu}\boldsymbol{n}\cdot(\partial_\mu \boldsymbol{n}\times\partial_\nu \boldsymbol{n}), \tag{2}$$

where $\boldsymbol{n}$ is the direction of the spin, u is an auxiliary coordinate, which together with τ parametrizes a disk. Multiple spins require a summation over spins and can be described by introducing a (dimensionless) spin density ρ_s

$$\sum_{\mathrm{impurities}} S_{\mathrm{WZ}} \to S = \int \mathrm{d}x \frac{\rho_s}{\xi_0} S_{\mathrm{WZ}}, \tag{3}$$

where ξ_0 is the underlying lattice constant for the spins.

Usually, two angular variables are used in parametrizing the spin $\mathbf{S} = s\,\{\sin(\theta)\cos(\psi), \sin(\theta)\sin(\psi), \cos(\theta)\}$:

$$\mathcal{L}_{\mathrm{WZ}}[\theta,\ \psi] = \frac{\mathrm{i}s\rho_s}{\xi_0}\cos\theta\,\partial_\tau\psi, \tag{4}$$

where we have neglected boundary contributions (topological terms).

The form of the Lagrangian equation (4) makes it difficult to separate fast and slow variables, since the angles θ and ψ contain both fast and slow modes. We need to find a different representation of the spin Berry phase, which will allow us to separate the fast and the slow modes explicitly. We first observe that the expression

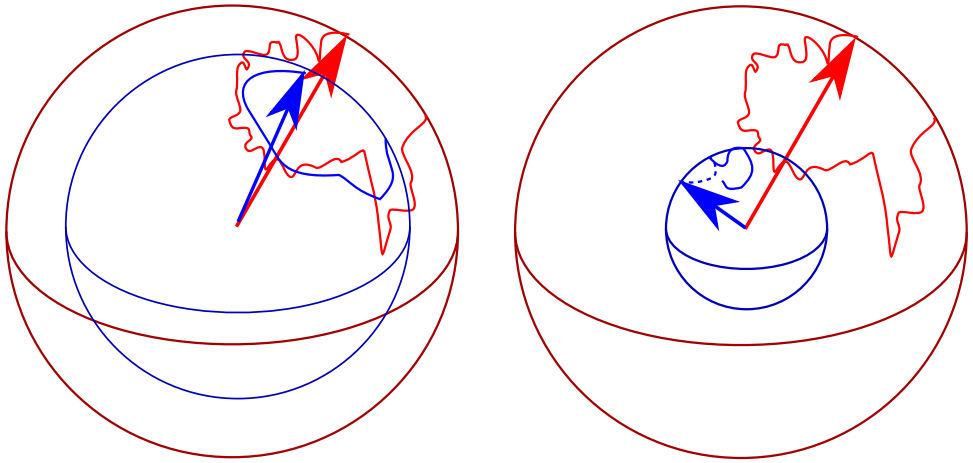

Figure 1. The fast (red) and slow (blue) spin trajectories as a function of time. The slow spin is shorter, since it is the fast spin averaged over some short timescale. The left panel shows the slow modes in the case of a free spin, in the right panel the spin physics is dominated by the interaction mediated by the backscattering electrons. In the latter case, the slow mode is orthogonal to the fast trajectory.

equation (4) can be obtained by considering a coordinate system comoving with the spin. Namely, we choose an orthnormal basis $\{\boldsymbol{e}_1, \boldsymbol{e}_2, \boldsymbol{e}_3\}$ at time $\tau = 0$ and assume that this coordinate system is comoving with the spin such that $s_i^e := (\boldsymbol{S}, \boldsymbol{e}_i)$ is independent of τ. Then it is easy to check that the following expression reproduces (4):

$$\mathcal{L}_{\mathrm{WZ}}[\theta, \psi] = -\frac{\mathrm{i}\rho_s}{2\xi_0}(\mathbf{S}, \mathbf{e}_i)(\mathbf{e}_j, \partial_\tau \mathbf{e}_k)\epsilon_{ijk}. \tag{5}$$

The check of equation (5) can be done by choosing the explicit parametrization

$$\mathbf{e}_1 = \{-\cos(\theta)\cos(\psi), -\cos(\theta)\sin(\psi), \sin(\theta)\}, \tag{6a}$$

$$\mathbf{e}_2 = \{\sin(\psi), -\cos(\psi), 0\}, \tag{6b}$$

$$\mathbf{e}_3 = \{\sin(\theta)\cos(\psi), \sin(\theta)\sin(\psi), \cos(\theta)\} = \boldsymbol{S}/s, \tag{6c}$$

with $\boldsymbol{S} \| \mathbf{e}_3$ and inserting equation (6) into equation (5). A specific choice of the basis $\mathbf{e}_{2,3}$ is not important since $\mathcal{L}_{\mathrm{WZ}}$ in the form equation (5) is manifestly covariant under both a rotation in x, y, z, and a change of basis $\{\mathbf{e}_i\}$.

In path integral quantization, we thus sum over all paths described by $\theta(x, \tau)$ and $\psi(x, \tau)$. The measure is given by $\mathcal{D}\{\Omega\} = \sin\theta \mathcal{D}\{\theta\}\mathcal{D}\{\psi\}$.

Let us now consider two superimposed spin motions: the actual trajectory considered in the path integral, and its slow component (figure 1). We already have the Wess–Zumino term for the actual trajectory. If we want to use equation (5) for the slow component, we need to introduce a second set of basis vectors which is comoving with the slow component. This doubles the number of angles, but we assume a separation of scales: of the four angles, two will be fast and two will be slow. Thus, there will be no double counting of modes which justifies our approach. A convenient choice for the slow basis is given by the rotation of the actual trajectory (figure 2)

$$\boldsymbol{e}_1' = -\sin(\alpha_\parallel)[\cos(\alpha_\perp)\mathbf{e}_1 + \sin(\alpha_\perp)\mathbf{e}_2] + \cos(\alpha_\parallel)\mathbf{e}_3, \tag{7a}$$

$$\boldsymbol{e}_2' = \sin(\alpha_\perp)\mathbf{e}_1 - \cos(\alpha_\perp)\mathbf{e}_2, \tag{7b}$$

$$\boldsymbol{e}_3' = \cos(\alpha_\parallel)[\cos(\alpha_\perp)\mathbf{e}_1 + \sin(\alpha_\perp)\mathbf{e}_2] + \sin(\alpha_\parallel)\mathbf{e}_3. \tag{7c}$$

The total path-integral measure now consists of the four angles: $\mathcal{D}\{\Omega_S, \Omega_{S'}\} = \cos\alpha_\parallel \sin\theta \mathcal{D}\{\theta\}\mathcal{D}\{\psi\}\mathcal{D}\{\alpha_\parallel\}\mathcal{D}\{\alpha_\perp\}$, which will be the product of the measures for fast and slow modes.

Now we can describe the dynamics of the slow modes, which is given by the slow Wess–Zumino term: we pick the bases such that $\mathbf{S} \| \mathbf{e}_3$ and $\mathbf{S}_{\mathrm{slow}} \| \mathbf{e}_3'$. The dynamics of the slow modes are then obtained by using equation (5) with the full spin $\mathbf{S}$ and the slow basis $\mathbf{e}_3'$:

$$S_{\mathrm{WZ}}^{\mathrm{slow}} = = \mathrm{i}s\rho_s\xi_0^{-1}\int \mathrm{d}x \int \mathrm{d}t \sin(\alpha_\parallel)[\partial_\tau\alpha_\perp + \cos(\theta)\partial_\tau\psi]. \tag{8}$$

The dynamics is that of the basis $\{\boldsymbol{e}_1', \boldsymbol{e}_2', \boldsymbol{e}_3'\}$ (i.e. of the slow spin), whereas the overall scale is that of the actual trajectory projected onto the slow component. This projection may be viewed as a renormalization of the length of the spin's slow component.

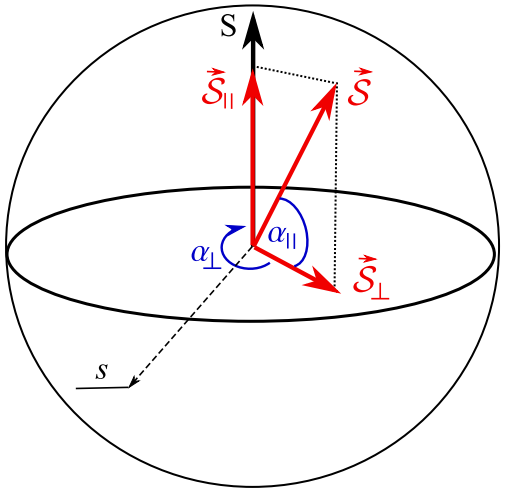

Figure 2. The parametrization of a spin by the angles θ, ψ, $\alpha_{\perp}$, $\alpha_{||}$.

2.2. The interaction between the spins and the fermions

The low-energy fermion modes are obtained by linearizing the spectrum and expanding the operators $\hat{c}$ in smooth chiral modes $\hat{R}_{\sigma}$, $\hat{L}_{\sigma}$

$$\hat{c}_{\uparrow\downarrow}(n) = \mathrm{e}^{-\mathrm{i}k_{\mathrm{F}}\xi_0 n}\hat{R}_{\uparrow\downarrow}(x) + \mathrm{e}^{\mathrm{i}k_{\mathrm{F}}\xi_0 n}\hat{L}_{\uparrow\downarrow}(x), \quad x = n\xi_0. \tag{9}$$

The Lagrangian density of the band electrons becomes

$$\mathcal{L}_{\mathrm{e}} = \Psi^{\dagger}[(\hat{I}\otimes\hat{I})\partial_{\tau} - \mathrm{i}(\hat{I}\otimes\hat{\tau}^{z})v_{\mathrm{F}}\partial_{x}]\Psi. \tag{10}$$

The first space in the tensor product is the spin one, the Pauli matrices $\hat{\tau}^{a}$ act in the chiral space; $\hat{I} = \mathrm{diag}(1,\,1)$; $v_{\mathrm{F}} = 2t\xi_0\sin(k_{\mathrm{F}}\xi_0)$ is the Fermi velocity; $\Psi^{\mathrm{T}} = (R_{\uparrow},\,R_{\downarrow},\,L_{\uparrow},\,L_{\downarrow})$ is the four-component fermionic spinor field. If the electron interaction is taken into account, it is more convenient to use the bosonized Lagrangian density

$$\mathcal{L}_{\mathrm{e}} = -\sum_{\rho=\mathrm{c,s}}\left\{\frac{\mathrm{i}}{\pi}\partial_x\Theta_{\rho}\partial_{\tau}\Phi_{\rho} - \frac{1}{2\pi}\left[u_{\rho}K_{\rho}(\partial_x\Theta_{\rho})^2 + \frac{u_{\rho}}{K_{\rho}}(\partial_x\Phi_{\rho})^2\right]\right\}, \tag{11}$$

where K_{ρ} is the Luttinger paramter; u_{ρ} the renormalized Fermi velocity; and we have used the bosonization identity

$$\psi_{r\sigma} = \frac{1}{\sqrt{2\pi\xi_0}}U_{\sigma}\mathrm{e}^{-\mathrm{i}rk_{\mathrm{F}}x}\mathrm{e}^{-\frac{\mathrm{i}}{\sqrt{2}}[r\Phi_{\mathrm{c}}-\Theta_{\mathrm{c}}+\sigma(r\Phi_{\mathrm{s}}-\Theta_{\mathrm{s}})]}. \tag{12}$$

Φ_{c} (Φ_{s}) and Θ_{c} (Θ_{s}) are dual bosonic fields belonging to the charge (spin) sector, r distinguishes right- and left-moving modes, σ is the spin projection and U_{σ} are Klein factors. One can introduce spin and charge sources to determine how the low energy degrees of freedom couple to external perturbations:

$$\mathcal{L}_{\mathrm{source}} = h_{\mathrm{c}}(\rho_{\mathrm{c}}^{R} + \rho_{\mathrm{c}}^{L}) + h_{\mathrm{s}}(\rho_{\mathrm{s}}^{R} - \rho_{\mathrm{s}}^{L}) = -\frac{\sqrt{2}\,h_{\mathrm{c}}}{\pi}\partial_x\Phi_{\mathrm{c}} + \frac{\sqrt{2}\,h_{\mathrm{s}}}{\pi}\partial_x\Theta_{\mathrm{s}}, \tag{13}$$

here $\rho_{\mathrm{c/s}}^{R/L} = \rho_{\uparrow}^{R/L} \pm \rho_{\downarrow}^{R/L}$ is the charge/spin density of the right-/left-moving electrons. The spin source is included for purely illustrative purposes. We will combine the fermionic and bosonic description, selecting the one which is most convenient for the given caculations.

Now consider the electron-spin interactions $\mathcal{H}_{\mathrm{int}}$. We will explicitely distinguish forward and backward scattering since they give rise to different physics. The slow part of the backscattering term is (see appendix)

$$\mathcal{L}_{\mathrm{int}}^{(\mathrm{sl,\,bs})} = \frac{s\cos(\alpha_{||})\rho_{\mathrm{s}}}{2}R^{\dagger}\left\{J_{\perp}\left[\mathrm{e}^{\mathrm{i}\psi}\sin^2\left(\frac{\theta}{2}\right)\hat{\sigma}^{-} - \mathrm{e}^{-\mathrm{i}\psi}\cos^2\left(\frac{\theta}{2}\right)\hat{\sigma}^{+}\right] + 2J_z\sin(\theta)\hat{\sigma}^{z}\right\}L\mathrm{e}^{-\mathrm{i}\alpha} + \mathrm{h.c.}, \tag{14}$$

where $\alpha = \alpha_{\perp} - 2k_{\mathrm{F}}x$ and we have introduced the spin-flip operator $S_{\pm} = S_x \pm \mathrm{i}S_y$.

For the forward scattering, we obtain

$$\mathcal{L}_{\rm int}^{(\rm sl,\,fs)} = \frac{s\sin(\alpha_\parallel)\rho_s}{2} R^\dagger \{J_\perp^{\rm f}\sin\theta\,[e^{i\psi}\sigma^- + e^{-i\psi}\sigma^+] + 2J_z^{\rm f}\cos\theta\sigma^z\}R + (R\to L) \tag{15}$$

3. Renormalization of forward versus backward scattering coupling constants

Equations (14) and (15) describe two competing phenomena: forward scattering tends towards Kondo-type physics, backward scattering opens a gap (see section 4). Both phenomena are distinct and mutually exclusive. If backscattering is dominant, then the emerging gap will cut the RG and suppress forward scattering. If forward scattering dominates, the formation of Kondo-singlett prevents the gap from opening [7]. We will focus on the physics related to the gaps. Therefore, we have to identify conditions under which the backscattering terms are more important. To determine the dominant term, we consider a first loop RG.

Let us consider the bosonized free electrons, equation (11). They constitute two Luttinger liquids, describing a spin density wave (SDW) and a charge density wave (CDW). If there is no electron–electron interaction, then $K_{\rm s} = K_{\rm c} = 1$. A weak, short range, spin independent repulsion between electrons changes $K_{\rm c}$ to $K_{\rm c} \lesssim 1$, but leaves $K_{\rm s}$ untouched.

The RG equations for the couplings read as (see appendix B):

$$\partial_l J_z^{\rm f} = -J_z^{\rm f},\ \ \partial_l J_\perp^{\rm f} = \left[\tfrac{1}{2}\left(K_{\rm s} + \tfrac{1}{K_{\rm s}}\right) - 2\right]J_\perp^{\rm f}, \tag{16}$$

$$\partial_l J_z^{\rm b} = \left[\tfrac{1}{2}(K_{\rm s}+K_{\rm c}) - 2\right]J_z^{\rm b},\ \partial_l J_\perp^{\rm b} = \left[\tfrac{1}{2}\left(K_{\rm c} + \tfrac{1}{K_{\rm s}}\right) - 2\right]J_\perp^{\rm b}, \tag{17}$$

where l parametrizes an energy cutoff Λ' via $\Lambda' = \exp(l)\Lambda$. The flow differs from that of single Kondo impurity because we consider a *dense array* of impurities. All of these terms are relevant, if $K_{\rm c}$ and $K_{\rm s}$ are close to 1. Assuming weak, short range, spin independent repulsion (i.e. $K_{\rm c} \lesssim 1$, and $K_{\rm s} = 1$), we see that the backward scattering terms flow faster in the RG-flow from high to low energies than forward scattering ones, i.e. the terms $\sim J^{\rm b}$ can dominate.

Let us assume that an impurity scatters anisotropically in spin space ($J_z \neq J_\perp$), but there is no difference between the electrons' directions ($J_{\rm bare}^{\rm f} = J_{\rm bare}^{\rm b}$). Then, simple scaling shows that backward scattering becomes relevant prior to forward scattering. The scattering will remain anisotropic and the strength of the anisotropy is dictated by the inital conditions (J_z versus $J_\perp$ at the beginning of the flow).

Weak, short range, spin dependent electron–electron interactions do not change the picture and backscattering dominates, provided that $|K_{\rm s} - 1| < |K_{\rm c} - 1|$. However, if the spin dependent electron–electron interactions are attractive (repulsive), they will drive the flow towards dominantly spin-flip (spin-conserving) backscattering.

Thus, we conclude that the gap physics dominates if there is a weak, repulsive, spin-independent electron–electron interaction. From now on, we consider this regime and neglect $J^{\rm f}$. We note that it is well-known that for large spins the Kondo-temperature is small [36]. Thus, for sufficiently large spins we can conclude without an explicit RG analysis that the gap physics will dominate.

4. Effects of backward scattering

We now focus on effects generated by backscattering. If the spin configuration is fixed, the backscattering terms act like mass terms for the fermions. This modifies the dispersion relations, as shown in figure 3. The ground state energy of single component massive fermions with mass m differs from that of gapless fermions by

$$\Delta E = -\frac{\xi_0}{2\pi v_{\rm F}} m^2 \ln(t/|m|) + \mathcal{O}(m^2). \tag{18}$$

To minimize the ground state energy, one thus has to maximize the gaps. Depending on the relative values of J^z and $J^\perp$ this leads to different ground state spin configurations and different physics.

4.1. EA anisotropy, $J_z \gg J_\perp$

Let us consider $J_z \gg J_\perp$. It is convenient to remove the phases α and ψ from the interaction equation (14). This can be done by the transformation of the fermion fields

$$R_\uparrow \to e^{-i\psi/2 - i\alpha/2}R_\uparrow,\quad R_\downarrow \to e^{i\psi/2 - i\alpha/2}R_\downarrow,\quad L_\uparrow \to e^{-i\psi/2 + i\alpha/2}L_\uparrow,\quad L_\downarrow \to e^{i\psi/2 + i\alpha/2}L_\downarrow, \tag{19}$$

which is anomalous. The anomaly is the well-known Tomonaga–Luttinger anomaly; its contribution to the Lagrangian is [37]

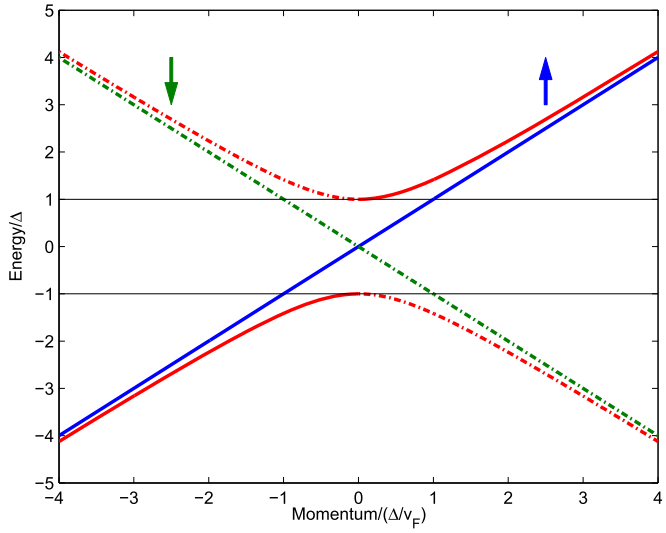

Figure 3. The dispersion of helical modes. Blue and green lines correspond to particles and holes of the first helical sector. For helical particles the direction is in one-to-one correspondes with their spin. Upon opening a gap Δ, the dispersion changes to the red curve.

$$\sum_{\sqrt{2}\Phi=\alpha,\psi} \mathcal{L}_{\mathrm{TL}}[\Phi, v_{\mathrm{F}}] = \sum_{\sqrt{2}\Phi=\alpha,\psi} \frac{1}{2\pi v_{\mathrm{F}}}[(\partial_\tau \Phi)^2 + (v_{\mathrm{F}}\partial_x \Phi)^2]. \tag{20}$$

This result may also be obtained from Abelian bosonization [38] (see the appendix C)[4]. We have neglected coupling between the charge (spin) density and the field α (ψ). This mixing is generically of the form

$$\mathcal{L}_{\mathrm{mixing}} \sim \mathrm{i}\partial_\tau \alpha(\rho_L - \rho_R)_{\mathrm{c}} + u\partial_x \alpha(\rho_L + \rho_R)_{\mathrm{c}} + \mathrm{i}\partial_\tau \psi(\rho_L + \rho_R)_{\mathrm{s}} + u\partial_x \psi(\rho_L - \rho_R)_{\mathrm{s}}, \tag{21}$$

where ρ_r stands for a density of left-/right-moving ($r = L$ and $r = R$) electrons and u is their velocity. Once the electrons become gapped, the low-energy degrees of freedom cannot excite density fluctuations. With this accuracy, in the low energy theory we can neglect derivatives of the electron densities.

The full Lagrangian is thus

$$\mathcal{L}^{(\mathrm{sl})} \simeq \mathcal{L}_{\mathrm{e}} + \mathcal{L}^{(\mathrm{sl})}_{\mathrm{int}}|_{\alpha,\psi=0} + \sum_{\sqrt{2}\Phi=\alpha,\psi} \mathcal{L}_{\mathrm{TL}}(\Phi, v_{\mathrm{F}}) + \mathcal{L}_{\mathrm{WZ}}; \tag{22}$$

Here $\mathcal{L}^{(\mathrm{sl})}_{\mathrm{int}}$ is only the backward scattering part $\mathcal{L}^{(\mathrm{sl,bs})}_{\mathrm{int}}$, equation (14). After the transformation equation (19), the sources now couple to the phases Φ_{c} and Θ_{s} and the angles

$$\mathcal{L}_{\mathrm{source}} = -\frac{h_{\mathrm{c}}}{\pi}\partial_x \alpha - \frac{h_{\mathrm{s}}}{\pi}\partial_x \psi - \frac{\sqrt{2}\,h_{\mathrm{c}}}{\pi}\partial_x \Phi_{\mathrm{c}} + \frac{\sqrt{2}\,h_{\mathrm{s}}}{\pi}\partial_x \Theta_{\mathrm{s}}. \tag{23}$$

$\mathcal{L}^{(\mathrm{sl})}_{\mathrm{int}}$ in equation (22) is a mass term. The masses for fixed spin variables are given by

$$m_{\pm}^2 = \frac{(s\cos\alpha_{\parallel}\rho_{\mathrm{s}})^2}{4}(\sqrt{(J_\perp^{\mathrm{b}})^2\cos^2\theta + (J_z^{\mathrm{b}})^2\sin^2\theta} \pm J_\perp^{\mathrm{b}})^2\,. \tag{24}$$

In the case of $J_z \gg J_\perp$ the gap is always large (of order J_z) and it is maximized for $\theta = \pi/2$ and $\alpha_{\parallel} = 0$.

Since all fermions are gapped we may neglect their coupling to external sources, provided we restrict ourselves to energies below the gap. We now integrate out the fermions under this assumption, i.e. we will consider correlation functions on length scales larger than the coherence length v_{F}/m. Since the original normalization of the path integral was with respect to gapless fermions, the effective Lagrangian is now changed by the fermionic ground state energy equation (18). The total Lagrangian reads as

$$\mathcal{L}^{(\mathrm{sl})} \simeq -\frac{\Delta E}{\xi_0} + \sum_{\sqrt{2}\Phi=\alpha,\psi} \mathcal{L}_{\mathrm{TL}}(\Phi, v_{\mathrm{F}}) + \mathcal{L}_{\mathrm{WZ}}, \tag{25}$$

where we also have assumed that fluctations of the angles θ and $\alpha_{\parallel}$ are small, such that the angles are close to their ground state values. ΔE is a function of the angles, see equations (18) and (24). Expanding equation (25) in $\theta' = \theta - \pi/2$ and $\alpha_{\parallel}$, we obtain

[4] We use the conventions from [39].

$$\mathcal{L}^{(\mathrm{sl})}_{(\mathrm{ea})} = \sum_{\sqrt{2}\Phi=\alpha,\psi} \mathcal{L}_{\mathrm{TL}}(\Phi,\, v_{\mathrm{F}}) + \underbrace{a\{[(J^{\mathrm{b}}_z)^2 - (J^{\mathrm{b}}_\perp)^2](\theta')^2 + [(J^{\mathrm{b}}_z)^2 + (J^{\mathrm{b}}_\perp)^2](\alpha_\parallel)^2\}}_{\mathcal{L}_{\mathrm{gs}}} + \mathrm{i}s\rho_{\mathrm{s}}\xi_0^{-1}\alpha_\parallel(\partial_\tau\alpha), \tag{26}$$

where $a = \log(t/J)(s\rho_{\mathrm{s}})^2/4\pi v_{\mathrm{F}}$, and we do not distinguish between the J's in the log. We will further assume for now that $\partial_\tau\psi$ is small, such that the cross-term $\alpha_\parallel\theta'\partial_\tau\psi$ is a higher order contribution. This will be verified below. $\mathcal{L}_{\mathrm{gs}}$ in equation (26) is the mass term for θ' and $\alpha_\parallel$, which shows that the assumption of small θ' and $\alpha_\parallel$ is consistent.

Now we perform the integrals over $\alpha_\parallel$ and θ' and obtain

$$\mathcal{L}^{(\mathrm{sl})}_{(\mathrm{ea})} = \sum_{\sqrt{2}\Phi=\alpha,\psi} \mathcal{L}_{\mathrm{TL}}(\Phi,\, v_{\mathrm{F}}) + \frac{(s\rho_{\mathrm{s}}\xi_0^{-1})^2}{4a\,((J^{\mathrm{b}}_z)^2 + (J^{\mathrm{b}}_\perp)^2)}(\partial_\tau\alpha)^2. \tag{27}$$

Note that ψ and α remain gapless, justifying the previous approximation of small $\partial_\tau\psi$. Thus, two angular modes are fast (θ and $\alpha_\parallel$) and two are slow (α and ψ), as we expected.

Equation (27) is the action of two $U(1)$-symmetric Luttinger liquids with a charge mode, α, and a spin mode, ψ

$$\mathcal{L}_{\mathrm{ea}} = \frac{1}{2}\mathcal{L}_{\mathrm{TL}}(\psi,\, v_{\mathrm{F}}) + \frac{1}{K_\alpha}\mathcal{L}_{\mathrm{TL}}(\alpha,\, v_\alpha). \tag{28}$$

The two phases couple to different sources: α to charges and ψ to spins. The slow mode α has a renormalized velocity and Luttinger parameter

$$\frac{v_\alpha}{v_{\mathrm{F}}} = \frac{K_\alpha}{2} \simeq \xi_0\frac{\sqrt{J_z^2 + J_\perp^2}}{\pi v_{\mathrm{F}}}\sqrt{\log(t/J)} \ll 1, \tag{29}$$

where we used that the band width is the largest energy scale (i.e. $v_{\mathrm{F}}/\xi_0 \gg J$) in the last inequality. This severly affects the charge transport, which is mediated by α.

4.2. Breaking the $\mathbb{Z}_2$ symmetry

We have demonstrated that for $J_z \gg J_\perp$, all fermionic modes have approximately the same gap $\sim J_z$. Approaching the $SU(2)$ symmtric point, the mass m_- shrinks until it would reach zero at $J_z = J_\perp$. In terms of the EA picture, some fermions (two helical modes) become light and their contribution encompasses large fluctuations on top of their ground state energy. We explicitely assumed that the fluctuations around the ground state are small. Therefore, our approach is no longer valid for $m_- \to 0$.

For now, let us consider the other limit $J_z \ll J_\perp$. We will see that this parameter regime behaves in a way qualitatively different to $J_z \gg J_\perp$. The order parameter distinguishing the phases is discussed in section 6. The vanishing of the gap for $J_z \to J_\perp$, the spontaneous symmetry breaking for $J_z \ll J_\perp$ and the presence of an order parameter all strongly suggest the presence of a quantum phase transition, although its theoretical description is missing.

4.3. EP anisotropy, $J_z \ll J_\perp$

Let us put for simplicity $J_z \to 0$. Then, it is convenient to express equation (14) through helical modes

$$\mathcal{L}^{(h_1)}_{\mathrm{bs}} = s\cos\alpha_\parallel\rho_{\mathrm{s}}[J_\perp R^\dagger_\uparrow \cos^2(\theta/2)\mathrm{e}^{-\mathrm{i}(\psi+\alpha)}L_\downarrow + \mathrm{h.c.}], \tag{30}$$

$$\mathcal{L}^{(h_2)}_{\mathrm{bs}} = -s\cos\alpha_\parallel\rho_{\mathrm{s}}[J_\perp R^\dagger_\downarrow \sin^2(\theta/2)\mathrm{e}^{\mathrm{i}(\psi-\alpha)}L_\uparrow + \mathrm{h.c.}]. \tag{31}$$

Clearly, the interesting points are $\theta = 0,\, \pi$ and $\theta = \pi/2$. If $\theta = \pi/2$, then the effective $J_\perp$ is reduced by a factor of $\cos^2\pi/4 = \sin^2\pi/4 = \frac{1}{2}$ relative to the effective $J_\perp$ of a single gapped helical sector at $\theta = 0,\, \pi$. Since the ground state energy equation (18) of a helical sectors with the gap m_i is

$$\Delta E_{\mathrm{hel}} = -\frac{\xi_0}{2\pi v_{\mathrm{F}}}m_i^2\ln(t/|m_i|) + \mathcal{O}(m_i^2), \quad m_i \sim J_\perp, \tag{32}$$

the ground state of a single gapped sector of twice the mass has a lower energy than that of two equally gapped helical sectors. Thus, it is energetically favorable to spontaneously break the $\mathbb{Z}_2$ symmetry between different helical sectors. The two ground states are labelled by $\theta = 0$ and $\theta = \pi$.

Let us choose $\theta = 0$. Then, the first helical sector equation (30) becomes gapped, while the second sector equation (31) is gapless. Now, the angle $\alpha - \psi$ does not enter the action if fluctuations of θ are set to zero. It enters (in the leading order in θ) only via the combination

$$\mathcal{L} \supset \underbrace{-s\cos\alpha_\parallel\rho_{\mathrm{s}}J_\perp\frac{\theta^2}{4}\mathrm{e}^{-\mathrm{i}(\alpha-\psi)}R^\dagger_\downarrow L_\uparrow + \mathrm{h.c.}}_{\mathcal{L}^{(H2)}_{\mathrm{bs}}} + \underbrace{\mathrm{i}s\rho_{\mathrm{s}}\xi_0^{-1}\sin(\alpha_\parallel)\frac{\theta^2}{2}\partial_\tau\alpha}_{\mathcal{L}^{\mathrm{slow}}_{\mathrm{WZ}}}. \tag{33}$$

The last summand is (for $\alpha_\parallel \approx 0$) beyond our accuracy and will be neglected. The influence of the first two summands may be estimated by integrating over $R_\downarrow$ and $L_\uparrow$. The resulting expression is

$$\mathcal{L} \supset \mathrm{Tr}\log\left[\begin{pmatrix} \mathrm{i}\omega + v_\mathrm{F}k & 0 \\ 0 & \mathrm{i}\omega - v_\mathrm{F}k \end{pmatrix}^{-1}\begin{pmatrix} \mathrm{i}\omega + v_\mathrm{F}k & s\cos\alpha_\parallel\rho_\mathrm{s}J_\perp\frac{\theta^2}{4}\mathrm{e}^{-\mathrm{i}(\alpha-\psi)} \\ s\cos\alpha_\parallel\rho_\mathrm{s}J_\perp\frac{\theta^2}{4}\mathrm{e}^{\mathrm{i}(\alpha-\psi)} & \mathrm{i}\omega - v_\mathrm{F}k \end{pmatrix}\right]. \tag{34}$$

The off-diagonal parts will enter only starting at the second order of the expansion of the log, thus $\alpha - \psi$ only enters with a prefactor of $J_\perp^2\theta^4$, which is smaller than our accuracy and has to be neglected. Under this assumption, the angle α can be shifted to $\alpha - \psi$, thus eliminating one angular variable, as the Wess–Zumino term equation (8) also depends only on $\alpha + \psi$ to leading order in θ and $\alpha_\parallel$. It is easiest to eliminate α by bosonizing the modes coupled to the spins, and shifting[5]

$$\Theta_\mathrm{s} \to \Theta_\mathrm{s} - \sqrt{2}\,\alpha/4, \quad \Phi_\mathrm{c} \to \Phi_\mathrm{c} + \sqrt{2}\,\alpha/4. \tag{35}$$

The shift needs to be in both spin and charge sectors such that all charge conserving fermionic bilinears of the gapless sector remain unaffected. This is a consequence of the helical nature of the sectors and means that α will couple to both spin and charge sources:

$$\mathcal{L}_\mathrm{source} \supset -\frac{h_\mathrm{c}}{2\pi}\partial_x\alpha - \frac{h_\mathrm{s}}{2\pi}\partial_x\alpha, \tag{36}$$

where we did not write the coupling of the sources to the fermions. Next, we integrate out the gapped helical sector. The ground state energy contribution from this is

$$\Delta E = -\frac{\xi_0}{2\pi v_\mathrm{F}}m^2\ln(t/|m|) + \mathcal{O}(m^2), \tag{37}$$

where $m^2 = \frac{1}{2}\left(s\rho_\mathrm{s}\cos\alpha_\parallel\cos\frac{\theta}{2}J_\perp\right)^2$. The ground state energy equation (37) is minimized for $\alpha_\parallel = 0$ (we remind that $\theta \approx 0$). We expand ΔE to second order in $\alpha_\parallel$ and θ and obtain

$$\Delta E \approx -(s\rho_\mathrm{s})^2\frac{\xi_0}{4\pi v_\mathrm{F}}\log(t/J_\perp)J_\perp^2[(\theta/2)^2 + (\alpha_\parallel)^2]. \tag{38}$$

Thus, θ and $\alpha_\parallel$ are high-energy modes, which confirms the consistency of our approach in the EP phase. We can integrate out the fast variables and obtain

$$\mathcal{L}_\mathrm{ep} = R_\downarrow^\dagger G_R^{-1}R_\downarrow + L_\uparrow^\dagger G_L^{-1}L_\uparrow + \frac{1}{K'_\alpha}\mathcal{L}_\mathrm{TL}(\alpha, v'_\alpha), \tag{39}$$

where

$$\frac{v'_\alpha}{v_\mathrm{F}} = \frac{K'_\alpha}{4} = \frac{\xi_0 J_\perp}{2\pi v_\mathrm{F}}\sqrt{\log(t/J_\perp)} \ll 1, \tag{40}$$

and $G_{R/L}^{-1} = \partial_\tau \mp \mathrm{i}v_\mathrm{F}\partial_x$ is the inverse Green's function of free helical fermions. Upon bosonization, the gapless helical fermions become a helical Luttinger liquid:

$$\mathcal{L} = \mathcal{L}_\mathrm{TL}(\Phi^{H1}, v_\mathrm{F}) + \frac{1}{K'_\alpha}\mathcal{L}_\mathrm{TL}(\alpha, v_\alpha). \tag{41}$$

Thus, the low energy physics is described by two $U(1)$ Luttinger liquids, just as in the EA case. However, the Luttinger liquids are now helical modes and they differ from the EA case in the way they couple to external sources (see equation (36)).

4.4. The effects of electron interactions

In the discussion of the EA and EP cases, we have neglected the effects of electron interactions. However, we used interactions to find the regime where the gap physics dominates Kondo physics. To fill this gap, we investigate the effects of interactions on the results of sections 4.1 and 4.3.

In the presence of interactions, K_s and/or K_c acquire values different from one. This changes the effect of the transformation equation (19) in the EA case. These transformations now induce terms of the form

$$\mathcal{L} \supset \frac{1}{2\sqrt{2}\,\pi}\left(\frac{u_\mathrm{c}}{K_\mathrm{c}}\partial_x\alpha\partial_x\Phi_\mathrm{c} - u_\mathrm{s}K_\mathrm{s}\partial_x\psi\partial_x\Theta_\mathrm{s}\right). \tag{42}$$

Since all the fermions become massive, these terms may be dropped (see discussion following equation (21)). The other effect of interactions is a renormalization of the gap m (equation (24)). This is simply a renormalization of the parameters appearing in equation (26), which we will neglect for now.

[5] The same may be done in the EA case, as explained in appendix C.

In the EP case, the situation is different, because one helical branch remains gapless. If $K_s \neq 1/K_c$, the Luttinger parameter and the velocity of a helical sector (e.g. $R_\downarrow$ and $L_\uparrow$ as one sector) are changed to

$$\tilde{K} = \sqrt{\frac{u_c K_c + \frac{u_s}{K_s}}{\frac{u_c}{K_c} + u_s K_s}}, \quad \tilde{u} = \frac{1}{2}\sqrt{u_c^2 + u_s^2 + u_c u_s K_c K_s + \frac{u_c u_s}{K_c K_s}}, \tag{43}$$

yielding the free part of the Lagrangian

$$\mathcal{L}_{h_i} = -\frac{\mathrm{i}}{\pi}\partial_x \Theta_{h_i}\partial_\tau \Phi_{h_i} + \frac{1}{2\pi}\left(\tilde{u}\tilde{K}(\partial_x \Theta_{h_i})^2 + \frac{\tilde{u}}{\tilde{K}}(\partial_x \Phi_{h_i})^2\right). \tag{44}$$

Here, Φ_{h_i} is the bosonic field belonging to a given helical sector. The helical sectors h_1 (consisting of $R_\uparrow$ and $L_\downarrow$) and h_2 (consisting of $R_\downarrow$ and $L_\uparrow$) couple as

$$\mathcal{L}_{h-h} = \frac{1}{2\pi}\left\{\left(u_c K_c - \frac{u_s}{K_s}\right)(\partial_x \Theta_{h_2}\partial_x \Theta_{h_1}) + \left(\frac{u_c}{K_c} - u_s K_s\right)(\partial_x \Phi_{h_2}\partial_x \Phi_{h_1})\right\} \tag{45}$$

The transformation equation (35) thus adds to the Lagrangian the new part

$$\delta\mathcal{L} = \frac{1}{4\pi}\left(\frac{u_c}{K_c} - u_s K_s\right)(\partial_x \Phi_{h_2}\partial_x \alpha) + \mathcal{O}(\partial\alpha\partial\Phi_{h_1}, \partial\alpha\partial\Theta_{h_1}), \tag{46}$$

where Φ_{h_2} is the bosonic field belonging to the gapless (helical) fermionic modes. Dropping once more couplings of the derivative of the density of a gapped fermion (from the first helical sector) to gapless modes, the total low-energy Lagrangian $\mathcal{L}_{ep}$ from equation (39) is modified only by $\delta\mathcal{L}$ in equation (46)[6]:

$$\mathcal{L}_{ep}^{int} = \mathcal{L}_{h_2} + \frac{1}{K'_\alpha}\mathcal{L}_{TL}(\alpha, v'_\alpha) + \delta\mathcal{L}. \tag{47}$$

This expression can be analyzed by rediagonalizing it in field space. To do so, first integrate out Θ_{h_2}. This yields

$$\begin{aligned}\mathcal{L}_{ep}^{int} = &\frac{1}{2\pi}\frac{1}{\tilde{u}\tilde{K}}(\partial_\tau \Phi_{h_2})^2 + \frac{1}{2\pi}\frac{\tilde{u}}{\tilde{K}}(\partial_x \Phi_{h_2})^2 + \frac{1}{2\pi}\left(\frac{1}{K'_\alpha}(\partial_\tau \alpha)^2 + \frac{1}{K'_\alpha}(v'_\alpha \partial_x \alpha)^2\right)\\ &+ \frac{1}{4\pi}\left(\frac{u_c}{K_c} - u_s K_s\right)\partial_x \alpha \partial_x \Phi_{h_2}.\end{aligned} \tag{48}$$

Next, we redefine the fields α and Φ_{h_2} such that the temporal derivatives have the same prefactor:

$$\alpha \to \sqrt{K'_\alpha}\,\alpha, \quad \Phi_{h_2} \to \sqrt{\tilde{u}\tilde{K}}\,\Phi_{h_2}. \tag{49}$$

This leads to

$$\mathcal{L}_{ep}^{int} = \frac{1}{2\pi}(\partial_\tau \Phi_{h_2})^2 + \frac{1}{2\pi}\tilde{u}^2(\partial_x \Phi_{h_2})^2 + \frac{1}{2\pi}(\partial_\tau \alpha)^2 + \frac{1}{2\pi}(v'_\alpha \partial_x \alpha)^2 + \delta\partial_x \alpha \partial_x \Phi_{h_2}, \tag{50}$$

where we have defined $\delta = \frac{1}{2\pi}\sqrt{\tilde{u}\tilde{K}K'_\alpha}\left(\frac{u_c}{K_c} - u_s K_s\right)$. Diagonalizing this leads to two new gapless particles with dispersion

$$\omega^2 = \tfrac{1}{2}(\tilde{u}^2 + v_\alpha^2 \pm \sqrt{(\tilde{u}^2 + v_\alpha^2)^2 + 4\delta^2})k^2. \tag{51}$$

Note that the remaining two degrees of freedom remain gapless. Interactions thus destroy the purely helical nature of low-energy excitations, but they cannot gap these exctiations.

4.5. Suppression of forward scattering

We have seen that dominant backscattering leads to a vacuum structure where $\alpha_\parallel \approx 0$. The forward scattering terms however are proportional to $\sin \alpha_\parallel$, equation (15). This confirms the suppression of their contribution once the gap is opened and examplifies our previous claim that Kondo physics and the gap physics are mutually exclusive.

5. Density–density correlation functions and disorder

5.1. Density–density correlation functions

We have shown that both the cases of EA and EP anistropy are described by two $U(1)$ Lutttinger liquids. However, the fields have different physical meaning as evinced by their coupling to external source. Their

[6] And a new effective Luttinger parameter and velocity, see equation (43).

difference can be seen from various correlation functions. Let us at first consider the density–density correlation function

$$\mathcal{C} = \langle \rho_c(1)\rho_c(2)\rangle = \frac{\delta^2 \log Z[h_c]}{\delta h_c(1)\delta h_c(2)}|_{h_c=0}, \tag{52}$$

where ρ_c is the electron density and $Z[h_c]$ is the generating functional in the presence of the source h_c. In general, there are several contributions to $\mathcal{C}$, including those from gapped and gapless excitations. Even if the fermionic modes become gapped, there still is a contribution from collective electron and spin modes to long range density–density correlation functions. This can be seen from the fact that some low energy degrees of freedom (EA: α; EP α and one helical fermion) couple to h_c. In Fourier space, the correlation functions are

$$\mathcal{C}_{ea}(\omega, q) = \left(\frac{q}{\pi}\right)^2 \langle \alpha^* \alpha\rangle, \tag{53}$$

$$\mathcal{C}_{ep}(\omega, q) = \left(\frac{q}{\pi}\right)^2 (\langle \Phi_H^* \Phi_H\rangle + \langle \alpha^*\alpha\rangle/4). \tag{54}$$

Using the corresponding low energy effective actions equations (28) and (39), this yields

$$\mathcal{C}_{ea}(\omega, q) = \frac{q^2 K_\alpha v_\alpha^2 \xi_0^{-2}}{\pi(\omega^2 + (v_\alpha q)^2)}, \tag{55}$$

$$\mathcal{C}_{ep}(\omega, q) = \frac{q^2}{\pi}\left(\frac{v_F^2 \xi_0^{-2}}{\omega^2 + (v_F q)^2} + \frac{1}{4}\frac{K'_\alpha v'^2_\alpha \xi_0^{-2}}{\omega^2 + (v'_\alpha q)^2}\right). \tag{56}$$

Equations (55) and (56) correspond to ideal metallic transport. The small Luttinger parameter of the bosonic modes (K_α, $K'_\alpha \ll 1$) reflects the coupling of the spin waves to the gapped fermions and leads to a reduced Drude weight [33].

5.2. The role of potential disorder

Let us investigate how potential disorder affects charge transport. We add a weak random potential

$$V_{dis} = g(x)\Psi^\dagger (I \otimes \tau^+)\Psi + \text{h.c.}, \tag{57}$$

where $g(x)$ is the smooth $2k_F$ component of the scalar random potential. Note that we have dropped quickly oscillating modes, just as for the spin impurities. If the disorder itself is distributed according to the Gaussion orthogonal ensemble, then its $2k_F$ component has a Gaussian unitary distribution. Thus the function g is drawn from a Gaussian unitary ensemble (GUE). We use $\langle g(x)\rangle = 0$ and $\langle g^*(x) g(y)\rangle = 2\mathcal{D}\delta(x-y)$. We assume that the potential disorder is sufficiently weak, such that it does not influence the high energy physics. The precise meaning of this statement will be specified later.

As first step, we integrate the disorder exactly by using the replica trick. Upon disorder-averaging we obtain

$$S_{dis} = \sum_{i,j}\int dx \int d\{\tau_{1,2}\}\mathcal{D}[(R^\dagger_{\uparrow i} L_{\uparrow i} + (\uparrow \leftrightarrow \downarrow))(x, \tau_1)(L^\dagger_{\uparrow j} R_{\uparrow j} + (\uparrow \leftrightarrow \downarrow))(x, \tau_2)], \tag{58}$$

where i, j are replica indices. The remainder of the action is diagonal in replica space.

To understand the effect of S_{dis} on transport we now have to integrate out the massive modes. Recall that this involves first a shift of the fermionic fields (equation (19))[7]:

$$S_{dis} = \int dx \int d\{\tau_{1,2}\}\mathcal{D}[(R^\dagger_{\uparrow i} L_{\uparrow i} e^{i\alpha_i} + (\uparrow \leftrightarrow \downarrow))(x, \tau_1)(L^\dagger_{\uparrow j} R_{\uparrow j} e^{-i\alpha_j} + (\uparrow \leftrightarrow \downarrow))(x, \tau_2)], \tag{59}$$

where the gapped and gapless modes now are cleanly separated in the rest of the action (with our accuracy). Thus, it is easy to integrate out the gapped modes. We treat S_{dis} perturbatively, obtaining an expansion in the parameter $\frac{\mathcal{D}}{v_F m} \ll 1$ (weak disorder).

In the EA case, all fermions are gapped and the only gapless mode appearing in $\mathcal{L}_{dis}$ is the charge mode α. In the EP case only the fermions with a given helicity (e.g. $R_\uparrow$ and $L_\downarrow$) become gapped and the disorder mixes the two helical Luttinger liquids (α and the fermions of the non-gapped helicity). It is convenient to treat EA and EP separately.

5.2.1. Easy axis

We start with the EA case, and put $J_\perp = 0$. For transparency, we choose the fermionic spin-dependent mass $m_{ea}(\uparrow / \downarrow) = \pm m$. The matrix Green's function for the fermions with a given spin reads:

[7] In EP, the shift leads to the same result after absorbing ψ in α.

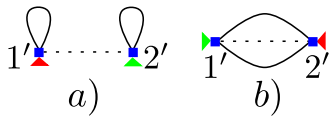

Figure 4. First order diagrams $O(\mathcal{D}^1)$ for the EA phase. Red (green) triangles denote $e^{i\alpha/2}$ ($e^{-i\alpha/2}$) with arguments of either the 1st or the 2nd vertex; dashed lines are the disorder correlation functions, solid lines stand for Green's functions of the massive fermions.

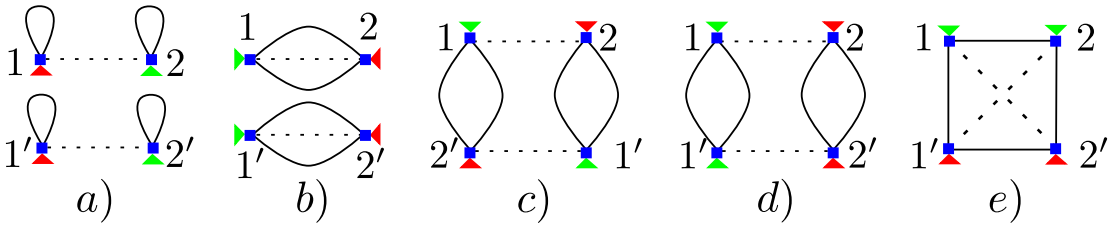

Figure 5. A relevant subset of the EA diagrams. Notations are explained in the caption of figure 4. (a) and (b) Class (ii), diconnected contributions. (c) Class (iii), red and green triangles are merged through a massive propagator. (d) Class (iv), we omit the diagram with crossed disorder lines. (e) Class (v), we omit the diagram with non-crossed disorder lines. Note that green and red triangles are connected by a massive propagator.

$$\hat{G}_m(\sigma) = ((G_R^{(0)})^{-1}(G_L^{(0)})^{-1} - m_{\rm ea}(\sigma)^2)^{-1}\begin{pmatrix} (G_L^{(0)})^{-1} & -m_{\rm ea}(\sigma) \\ -m_{\rm ea}(\sigma) & (G_R^{(0)})^{-1} \end{pmatrix}; \tag{60}$$

where $G_{R,L}^{(0)}$ are the Green's functions of free chiral particles. It is important that $\hat{G}_m$ is short ranged and it decays beyond the time scale $1/m_{\rm ea}$ (or beyond the coherence length $\xi_{\rm ea} \equiv v_f/m_{\rm ea}$). This implies in particular that two slow operators connected by a massive propagator form a single local operator on length- and timescales large compared to the inverse gap.

Leading terms are given by $\langle S_{\rm dis}\rangle_m$ where brackets mean that the massive fermions are integrated out. The corresponding diagrams are shown in figure 4. It is easy to check that the diagrams from figure 4(a) cancel out after summation over spin indices because $m_{\rm ea}(\uparrow) = -m_{\rm ea}(\downarrow)$. The diagrams from figure 4(b) are trivial since $\hat{G}_m$ is diagonal in the replica space and the spin phase α is smooth on the scale $1/m_{\rm ea}$; therefore

$$e^{i\alpha[1]}e^{-i\alpha[2]} \simeq e^{i\alpha[1]-i\alpha[1]} = 1, \tag{61}$$

with some small gradient corrections which are unable to yield pinning. Here we denoted $\alpha[j] \coloneqq \alpha(x_1, \tau_1)$.

Sub-leading terms of the order of $\frac{\mathcal{D}^2}{v_F m}$ are given by $\langle S_{\rm dis}S_{\rm dis}\rangle$. To be explicit, we need to compute

$$\begin{aligned}\langle S_{\rm dis}S_{\rm dis}\rangle_{\rm EA} = \mathcal{D}^2\Big\langle \int {\rm d}\{x, x'; \tau_{1,2}, \tau'_{1,2}\} \\ \times [(R^\dagger_{\uparrow i}L_{\uparrow i}e^{i\alpha_i} + (\uparrow \leftrightarrow \downarrow))(x,\tau_1)(L^\dagger_{\uparrow j}R_{\uparrow j}e^{-i\alpha_j} + (\uparrow \leftrightarrow \downarrow))(x,\tau_2)] \\ \times [(R^\dagger_{\uparrow k}L_{\uparrow k}e^{i\alpha_k} + (\uparrow \leftrightarrow \downarrow))(x',\tau'_1)(L^\dagger_{\uparrow l}R_{\uparrow l}e^{-i\alpha_l} + (\uparrow \leftrightarrow \downarrow))(x',\tau'_2)]\Big\rangle_{\rm EA}.\end{aligned} \tag{62}$$

In order to pin the CDW (the field α), an operator evaluating α at different times (i.e. times further apart than $1/m_{\rm ea}$) has to survive. The correlation function $\langle S_{\rm dis}S_{\rm dis}\rangle_{\rm EA}$ contains various possible contractions, most of which are unable to generate pinning:

(i) Contractions involving two fermionic creation or annihilation operators: they vanish due to the structure of the fermionic Green's function, which does not allow for propagation of Cooper pairs.

(ii) Contractions which simplify to two copies of the first order contribution (see figures 5(a), (b)): they do not generate backscattering, as shown above.

(iii) Contractions of fermions at (x, τ_1) with fermions at (x', τ'_2) and of fermions at (x, τ_2) with fermions at (x', τ'_1), with no contractions between (x, τ_1) and (x', τ'_1) (figure 5(c)): in these contractions—due to the short range nature of the fermions' Green'(s) functions—$e^{i\alpha}$ fuses with $e^{-i\alpha}$ at the same position and time (at an accuracy of $1/m$), and thus generate only derivatives of α, which are unable to pin the CDW.

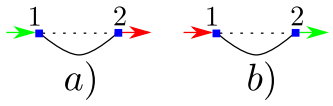

Figure 6. Two typical examples of first order diagrams $O(\mathcal{D}^1)$ for the EP phase. Red (green) arrows denote the product of smooth fields L, R with $e^{i\alpha/2}$ ($e^{-i\alpha/2}$). The smooth fields L, R are taken from the non-gapped helical sector.

(iv) Contractions of fermions at (x, τ_1) with fermions at (x', τ_1') and of fermions at (x, τ_2) with fermions at (x', τ_2'), with no contractions between (x, τ_1) and (x', τ_2') (figure 5(d)): these contractions all give the same result and are able to generate pinning.

(v) Contractions between all positions and times (figure 5(e)): this sets all positions and times (and replica indices) of the CDW equal to each other (with accuracy $1/m$), such that again only derivatives of the field α survive.

We calculate only one typical diagram which survives after all summations and is able to generate pinning (type (iv)). An example of such a diagram is shown in figure 5(d). All other diagrams of class (iv) yield identical results. The sign of the mass does not matter as there is an even number of propagators for each species.

Neglecting unimportant numerical factors, the analytical expression for the diagram from figure 5(d) reads as:

$$D_{\mathrm{ea}}^{(2)} \propto \mathcal{D}^2 \sum_{i,j} \int \mathrm{d}\{x, x'; \tau_{1,2}, \tau_{1,2}'\}\, e^{2i(\alpha_i[\mathbf{1}]-\alpha_j[\mathbf{2}])} [\hat{G}_m(\mathbf{1}, \mathbf{1}')]_{1,2} \times [\hat{G}_m(\mathbf{1}', \mathbf{1})]_{1,2} [\hat{G}_m(\mathbf{2}, \mathbf{2}')]_{1,2} [\hat{G}_m(\mathbf{2}', \mathbf{2})]_{1,2}. \tag{63}$$

Here, we have taken into account that the diagonal structure of $\hat{G}_m$ results in $i = k$; $j = l$ and fused together slow spin phases, for instance: $\alpha[\mathbf{1}] + \alpha[\mathbf{1}'] \simeq 2\alpha[\mathbf{1}]$. Now we note that $\hat{G}_m(\mathbf{1}, \mathbf{1}') = \hat{G}_m(\mathbf{1} - \mathbf{1}')$ and integrate over all primed variables:

$$D_{\mathrm{ea}}^{(2)} \propto \frac{\tilde{\mathcal{D}}_0}{\xi_{\mathrm{ea}}^2} \sum_{i,j} \int \mathrm{d}\{x; \tau_{1,2}\}\, e^{i(\alpha_i[\mathbf{1}]-\alpha_j[\mathbf{2}])}; \quad \tilde{\mathcal{D}}_0 \equiv \mathcal{D}\left(\frac{\mathcal{D}}{v_{\mathrm{F}} m_{\mathrm{ea}}}\right). \tag{64}$$

The structure of equation (64) corresponds to the non-local Sine-Gordon model which appears in the theory of the usual disordered TLL [39]. The effective disorder strength $\tilde{\mathcal{D}}$ is renormalized and obeys the well-known RG equation [40]:

$$\mathrm{EA}: \partial_{\log} \log(\tilde{\mathcal{D}}) = 3 - 2K_\alpha \simeq 3, \quad \tilde{\mathcal{D}}(\xi_{\mathrm{ea}}) = \tilde{\mathcal{D}}_0; \tag{65}$$

the second equality of equation (65) has been obtained by using equation (29).

Note that the effective strength of the disorder is suppressed compared to free fermions by an additional factor of $\mathcal{D}/(v_{\mathrm{F}} m)$. However, the operator is more relevant than for free fermions, as $K_\alpha^{(\mathrm{EA})} \ll 1$.

5.2.2. Easy plane

Let us now turn to the EP case. We start again from the leading diagrams generated by $\langle S_{\mathrm{dis}} \rangle$. The principal difference of the EP phase from the EA one is that the matrix Green's function, equation (60), corresponds now to the massive fermions with a given helicity. This changes the structure of the first order diagram, see figure 6. All these diagrams correspond to forward-scattering of the massless helical fermions and they contain only small gradients of the phase α, see equation (61) and its explanation. Thus, the leading diagrams are trivial and they cannot yield localization, the sub-leading diagrams must be considered.

There are several categories of sub-leading diagrams:

(i) Contractions involving two creation or annihilation operators: they are identically zero.

(ii) Contractions which correspond to two copies of the leading diagrams (figure 7(a)): they do not lead to backscattering and cannot pin the charge transport.

(iii) Contractions of fermions at (x, τ_1) with fermions at (x', τ_2') and of fermions at (x, τ_2) with fermions at (x', τ_1'), with no contractions between (x, τ_1) and (x', τ_1') (the second part—excluding certain contractions—is trivial, as there is only one massive fermion at each vertex) (figure 7(b)): these contractions—due to the short range nature of the fermions' Green's function—combine $e^{i\alpha}$ with $e^{-i\alpha}$ at the same position and time (at an accuracy of $1/m$), and thus generate only derivatives of α, which are unable to pin the CDW.

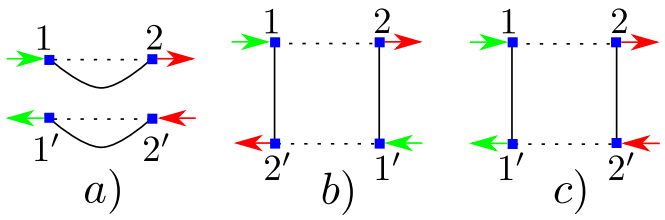

Figure 7. A relevant subset of the EP diagrams. Notations are explained in the caption of figure 6. (a) Class (ii), diconnected contributions. (b) Class (iii), red and green arrows are merged through a massive propagator. We omit the diagram with crossed disorder lines. Note that green and red arrows are connected by a massive propagator. (c) Class (iv), we omit the diagram with crossed disorder lines.

(iv) Contractions of fermions at (x, τ_1) with fermions at (x', τ_1') and of fermions at (x, τ_2) with fermions at (x', τ_2'), with no contractions between (x, τ_1) and (x', τ_2') (the second condition is again trivially satisifed) (figure 7(c)). These contractions all give the same result and are able to generate pinning.

The only relevant diagrams are those of class (iv), which all yield the same result. We will compute one of these diagrams (figure 7(c)). Neglecting unimportant numerical factors, the analytical expression for the diagram from figure 7(c) reads as:

$$D_{\rm ep}^{(2)} \propto \mathcal{D}^2 \sum_{i,j} \int \mathrm{d}\{x, x'; \tau_{1,2}, \tau_{1,2}'\} \mathrm{e}^{\mathrm{i}(\alpha_i[\mathbf{1}]-\alpha_j[\mathbf{2}])} L_{\downarrow j}^\dagger[\mathbf{2}] R_{\uparrow i}^\dagger[\mathbf{1}] L_{\downarrow i}[\mathbf{1}] R_{\uparrow j}[\mathbf{2}] [\hat{G}_m(\mathbf{1}, \mathbf{1}')]_{1,2} [\hat{G}_m(\mathbf{2}, \mathbf{2}')]_{1,2}; \quad (66)$$

see explanations after equation (63) and note the m must be substituted for $m_{\rm ea}(\sigma)$ in $\hat{G}_m$. Calculating integrals over all primed variables, we find:

$$D_{\rm ep}^{(2)} \propto \bar{\mathcal{D}}_0 \sum_{i,j} \int \mathrm{d}\{x; \tau_{1,2}\} \mathrm{e}^{\mathrm{i}(\alpha_i[\mathbf{1}]-\alpha_j[\mathbf{2}])} L_{\downarrow j}^\dagger[\mathbf{2}] R_{\uparrow i}^\dagger[\mathbf{1}] L_{\downarrow i}[\mathbf{1}] R_{\uparrow j}[\mathbf{2}], \quad \bar{\mathcal{D}}_0 \equiv \mathcal{D}\left(\frac{\mathcal{D}}{v_{\rm F} m}\right). \quad (67)$$

This equation also can be reduced to the form of equation (64) if remaining fermions are bosonized and we explicitly single out new CDWs and SDWs. However, the RG equation for $\bar{\mathcal{D}}$ can be obtained without such a complicated procedure with the help of the power counting. Firstly we note that the scaling dimension of each back-scattering term in equation (67), $L^\dagger R$ and $R^\dagger L$, is 1. The anomalous dimension of each exponential, $\mathrm{e}^{\pm \mathrm{i}\alpha}$, is $K_\alpha' \ll 1$. The normal dimension in equation (67) is 3 which comes from three-fold integral. Combining these dimensions together and neglecting small K_α', we find

$$\mathrm{EP}: \partial_{\log} \log(\bar{\mathcal{D}}) = 3 - 2 \times 1 + O(K_\alpha) \simeq 1; \quad \bar{\mathcal{D}}(\xi_{\rm ep}) = \bar{\mathcal{D}}_0, \ \xi_{\rm ep} = v_{\rm F}/m. \quad (68)$$

Note that while the scaling of the disorder strength is the same as for free fermions, but the effective strength (the starting value of the flow) is reduced parametrically by a factor of $\mathcal{D}/(v_{\rm F} m) \ll 1$.

5.2.3. Localization radius

We now can find the localization radius for both phases, EA and EP. The solution of the RG equations, equations (65) and (68), reads as

$$\tilde{\mathcal{D}}(x) = \tilde{\mathcal{D}}_0 \left(\frac{x}{\xi_{\rm ea}}\right)^3, \quad \bar{\mathcal{D}}(x) = \bar{\mathcal{D}}_0 \frac{x}{\xi_{\rm ep}}; \quad (69)$$

with $\xi_{\rm ep} = v_{\rm F}/m$. The localization radius is defined as a scale on which the renormalized disorder becomes of the order of the cut-off:

$$\tilde{\mathcal{D}}(L_{\rm ea}^{\rm (loc)}) = K_\alpha v_\alpha^2/\xi_{\rm ea} \sim K_\alpha^3 v_{\rm F}^2/\xi_{\rm ea}; \quad \bar{\mathcal{D}}(L_{\rm ep}^{\rm (loc)}) = v_{\rm F}^2/\xi_{\rm ep}. \quad (70)$$

The additional small factor K_α in the equation for $L_{\rm ea}^{\rm (loc)}$ can be justified with the help of the standard optimization procedure [39] where $L^{\rm (loc)}$ is defined as a spatial scale on which the typical potential energy of the disorder becomes equal to the energy governed by the term $\propto(\partial_x \alpha)^2$ in the Lagrangian $\mathcal{L}_{\rm ea}$, equation (28).

Definitions equation (70) result in

$$L_{\rm ea}^{\rm (loc)} \sim \xi_{\rm ea} K_\alpha \left(\frac{v_{\rm F}^2}{\xi_{\rm ea} \tilde{\mathcal{D}}_0}\right)^{1/3} \sim \xi_{\rm ea} K_\alpha \left(\frac{v_{\rm F} m_{\rm ea}}{\mathcal{D}}\right)^{2/3}; \quad L_{\rm ep}^{\rm (loc)} \sim \frac{v_{\rm F}^2}{\bar{\mathcal{D}}_0} \sim \xi_{\rm ep} \left(\frac{v_{\rm F} m}{\mathcal{D}}\right)^2. \quad (71)$$

Assuming $\xi_{ea} \sim \xi_{ep}$ and $m_{ea} \sim m$, we obtain

$$\frac{L_{ea}^{(loc)}}{L_{ep}^{(loc)}} \sim K_\alpha \left(\frac{\mathcal{D}}{v_F m}\right)^{4/3} \ll 1. \tag{72}$$

This demonstrates that the strong suppression of localization can occur in the EP phase where the helical symmetry is broken.

We note that the scaling exponent of $\tilde{\mathcal{D}}(x)$ is the same as in the case of non-interacting 1d fermions but suppression of localization in the EP phase is reflected by the additional large factor $v_F m/\mathcal{D}$ in the expression for the localization radius $L_{ep}^{(loc)}$. We further note that unlike for free fermions our flow starts at the correlation length v_F/m, not at the lattice constant ξ_0. However, for characteristic length scales $\xi_0 < l < \xi_{ea/ep}$, the mass is not relevant and the flow of our system mimics that of free fermions in the absence spinful impurities. The flow only begins to differ at $l \approx \xi_{ea/ep}$, such that we should compare to free fermions with a cutoff $\xi_{ea/ep}$.

5.2.4. Alternative approach to disorder

In this section we present an alternative approach which confirms the previous results on disorder. The main idea is to integrate out the massive modes before averaging over disorder. We will focus on the main steps and neglect unimportant prefactors. Let us start again at equation (57). In the EA case, we perform a shift $\Phi_c \to \Phi_c - \alpha/\sqrt{2}$. This shift leads to

$$V_{dis}^{ea} = g(x) e^{i\alpha} \Psi^\dagger (I \otimes \tau^+) \Psi + \text{h.c.}, \tag{73}$$

such that the field α couples to the potential disorder. Let us integrate out the massive fermions. The leading term (in powers of the disorder) in the Lagrangian is then

$$L_{dis} \sim \tfrac{1}{\xi_0} \int dx \, [g_{eff}(x) e^{i2\alpha} + \text{h.c.}], \tag{74}$$

where we introduced the non-Gaussian effective disorder

$$g_{eff}(x) \sim \frac{1}{2v_F} \int dy g(x + y/2) g(x - y/2) e^{-m|y|/v_F}; \tag{75}$$

the exponential stems from real space Green's function of fermions with mass m[8]. Equation (75) is valid for large distances $y \gg v_F/m$.

In the EP case, before integrating out the massive fermions, we shift their phase Φ_c by $\sqrt{2}\,\alpha/4$:

$$V_{dis}^{ep} = \int dx \, [g(x) e^{i\alpha/2} R_\uparrow^\dagger L_\uparrow + g(x) e^{i\alpha/2} R_\downarrow^\dagger L_\downarrow + \text{h.c.}]. \tag{76}$$

Each term describes a coupling of a gapped fermion from the first helical sector with a gapless one from the second helical sector and with a low-energy angle α. Upon integrating out the gapped fermions, the disorder generates the following contribution to the low energy effective Lagrangian:

$$\mathcal{L}_{dis}^{(H2)} \supset \int dx \, [g_{eff}(x) R_\downarrow^\dagger e^{i\alpha} L_\uparrow + \text{h.c.}], \tag{77}$$

where $g_{eff}(x)$ is of the form of equation (75)[9].

Thus, both in EA and EP, we obtain gapless particles coupled to an effective disorder.

To order $\frac{\mathcal{D}}{v_F m}$, only the first and second moment of the distribution function of g_{eff} contribute (see appendix E). This is equivalent to the statement that the non-Gaussianities of the distribution of g_{eff} are irrelevant in our approximation.

The leading order contributions of the effective disorder to the localization may then be estimated similarly to the diagrammatic approach. Upon integrating over the disorder (and assuming it is a Gaussian distribution), we obtain

$$S_{dis} \sim \sum_{i,j} \int d\tau d\tau' dx \frac{\mathcal{D}^2}{v_F m} \mathcal{O}_i(x, \tau) \mathcal{O}_j^\dagger(x, \tau'), \tag{78}$$

where the operator $\mathcal{O}$ is given by

$$\text{EA}: \ \mathcal{O}_i(x, \tau) = \frac{1}{\xi_0} e^{i2\alpha_i(x,\tau)}, \tag{79}$$

[8] Note that equation (74) corresponds to figures 5(c) and (d): the fermionic lines are contracted to a single point and the two disorder lines are merged into one line corresponding to g_{eff}.

[9] Equation (77) corresponds to contracting the internal fermion lines in figures 7(b) and (c), and then merging the two disorder lines into a single lines described by g_{eff}.

$$\text{EP}: \ \mathcal{O}_i(x,\tau) = e^{i\alpha_i} R^{\dagger}_{i,\downarrow} L_{i,\uparrow}. \tag{80}$$

This yields the same scaling and, thus, the same localization radius equation (71) as in the diagrammatic approach.

The advantage of this approach is that the order of approximations follows the ordering of the relevant energy scales. We first eliminate the highest energy (m) and only then approach the much smaller pinning energy. The price is the non-Gaussianity of the effective disorder. However, since higher moments of the effective disorder are suppressed by additional factors of $\frac{\mathcal{D}}{v_F m}$, the non-Gaussianities only enter in higher orders that we do not consider here.

6. Spin correlation functions and order parameter

Let us consider the spin correlators $\langle S^a(1) S^b(2)\rangle$ and see which correlation function reflects the broken $\mathbb{Z}_2$ symmetry.

Before computing the correlators, we note the following: the low energy physics of both phases is captured by two uncorrelated $U(1)$ Luttinger liquids and by a set of fast angles. The slow component of the spins (in the basis where $S_{\text{slow}} \| e_3'$) depends on the angles via

$$S^x/s = -\cos\alpha_\parallel \cos\alpha_\perp \cos\theta\cos\psi + \cos\alpha_\parallel \sin\alpha_\perp \sin\psi + \sin\alpha_\parallel \sin\theta\cos\psi; \tag{81a}$$

$$S^y/s = -\cos\alpha_\parallel \cos\alpha_\perp \cos\theta\sin\psi - \cos\alpha_\parallel \sin\alpha_\perp \cos\psi + \sin\alpha_\parallel \sin\theta\sin\psi; \tag{81b}$$

$$S^z/s = \cos\alpha_\parallel \cos\alpha_\perp \sin\theta + \sin\alpha_\parallel \cos\theta. \tag{81c}$$

The effective low energy physics is generated at $\alpha_\parallel \approx 0$. Therefore, equation (81) simplifies to

$$S^x/s = -\cos\alpha_\perp \cos\theta\cos\psi + \sin\alpha_\perp \sin\psi; \tag{82a}$$

$$S^y/s = -\cos\alpha_\perp \cos\theta\sin\psi - \sin\alpha_\perp \cos\psi; \tag{82b}$$

$$S^z/s = \cos\alpha_\perp \sin\theta; \tag{82c}$$

where we neglect fast fluctuations of $\alpha_\parallel$ around its ground state value. We will also need the correlation functions (for large distances) in a Luttinger liquid described by the field ρ with Luttinger parameter K and velocity v:

$$\langle \sin(\rho(x_1) \pm \rho(x_2))\rangle = 0; \quad \langle \cos(\rho(x_1) + \rho(x_2))\rangle = 0; \ \langle \sin(\rho(x_1))\cos(\rho(x_2))\rangle = 0; \tag{83a}$$

$$\langle \sin(\rho(x_1))\sin(\rho(x_2))\rangle = \langle \cos(\rho(x_1))\cos(\rho(x_2))\rangle = \frac{1}{2}\langle \cos(\rho(x_1) - \rho(x_2))\rangle = \frac{\xi_0^{K/2}}{[(v\tau + \xi_0)^2 + x^2]^{K/4}}. \tag{83b}$$

Here, $\langle \cos(\rho(x_1) + \rho(x_2))\rangle = 0$ due to 'electroneutrality' [39].

6.1. Spin correlation functions; EA

In the case of the EA anisotropy, the physics at energies smaller that $J_z - J_\perp$ is governed by $\theta \approx \pi/2$ (fast fluctuations are again neglected). At these energies the spin components become

$$S^x/s = \sin\alpha_\perp \sin\psi, \ \ S^y/s = -\sin\alpha_\perp \cos\psi, \ \ S^z/s = \cos\alpha_\perp. \tag{84}$$

Then the transverse spin correlators are given by

$$\langle S^x(1) S^x(2)\rangle/s^2 = \langle S^y(1) S^y(2)\rangle/s^2 = \langle (\sin\alpha_\perp \sin\psi)(1)(\sin\alpha_\perp \sin\psi)(2)\rangle + \mathcal{O}(\theta - \pi/2, \alpha_\parallel), \tag{85}$$

where (j) denotes (τ_j, x_j). Since ψ and α are not correlated, the correlation function factorizes. The correlation function of the $\alpha_\perp$ component can be written as

$$\langle \sin\alpha_\perp(1)\sin\alpha_\perp(2)\rangle = -\frac{1}{2}[\langle \cos(2k_F(x_1 + x_2) + \alpha(1) + \alpha(2))\rangle - \langle \cos(2k_F(x_1 - x_2) + \alpha(1) - \alpha(2))\rangle]. \tag{86}$$

Combining equations (86) and (83) leads to

$$\langle S^x(1) S^x(2)\rangle/s^2 = \frac{1}{4}\cos[2k_F(x_1 - x_2)]\langle \cos(\alpha(1) - \alpha(2))\rangle \langle \cos(\psi(1) - \psi(2))\rangle = \cos(2k_F x)\left(\frac{\xi_0}{\sqrt{(\tau v_\alpha)^2 + x^2}}\right)^{\frac{K_\alpha}{2}} \left(\frac{\xi_0}{\sqrt{(\tau v_F)^2 + x^2}}\right)^{\frac{1}{2}}, \tag{87}$$

where we introduced $x = x_1 - x_2$ and $\tau = \tau_1 - \tau_2$. The transverse spin correlation function of x and y components is

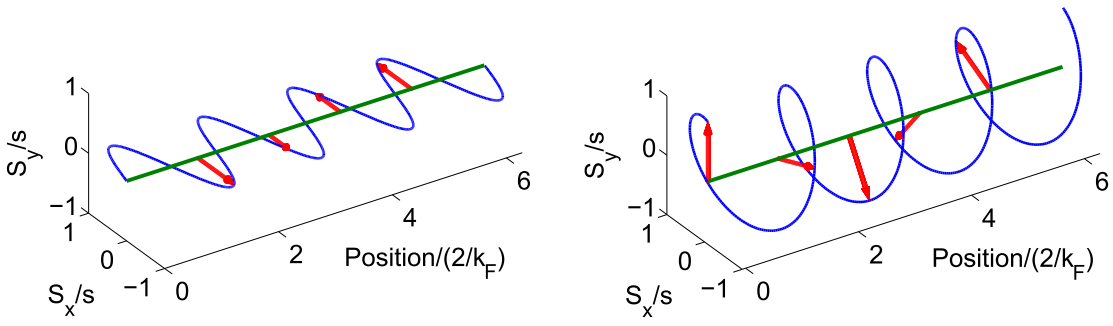

Figure 8. A travelling spin wave in the EA (left) and EP (right) setup. Since S^x and S^y in the EA case are uncorrelated to leading order, we only show one contribution.

$$\langle S^x(1)S^y(2)\rangle/s^2 \sim f(\alpha_\perp)\langle \sin\psi(1)\cos\psi(2)\rangle = 0. \tag{88}$$

Equation (88) shows that there is no spin rotation in xy-plane, see figure 8. In particular, this implies that the Fourier-transform of the dynamical in-plane spin susceptibility

$$\langle S^+(1)S^-(2)\rangle/s^2 = 2\langle S^x(1)S^x(2)\rangle/s^2, \tag{89}$$

has peaks both at $2k_F$ and $-2k_F$.

The correlators of S^z spin components are given by

$$\begin{aligned}\langle S^z(1)S^z(2)\rangle/s^2 &= \langle(\cos\alpha_\perp)(1)(\cos\alpha_\perp)(2)\rangle + \mathcal{O}(\theta-\pi/2,\,\alpha_\parallel)\\ &= \cos(2k_Fx)\left(\frac{\xi_0}{\sqrt{(\tau v)^2+x^2}}\right)^{\frac{K_\alpha}{2}}.\end{aligned} \tag{90}$$

They decay more slowly than the transverse spin correlator equation (88) because the S_z component couples more strongly to the localized electrons. The correlation function between the axis and the plane $\langle S^zS^x\rangle$ vanishes. Thus, all cross-correlation functions are zero in the EA case.

6.2. Spin correlation functions; EP

In the case of the EP, the asymptotics of the spin correlation functions are determined by $\theta \approx 0$, or $\theta \approx \pi$. Let us choose $\theta = 0$. Then the spin operators become

$$S^x/s = -\cos\alpha_\perp\cos\psi + \sin\alpha_\perp\sin\psi = -\cos(\alpha_\perp+\psi); \tag{91}$$

$$S^y/s = -\cos\alpha_\perp\sin\psi - \sin\alpha_\perp\cos\psi = -\sin(\alpha_\perp+\psi); \tag{92}$$

$$S^z/s = 0. \tag{93}$$

In our notations: $\alpha_\perp = 2k_Fx + \alpha$ and $\alpha \to \alpha - \psi$ in the EP case. Thus, the transverse spin correlation function reads as

$$\begin{aligned}\langle S^x(1)S^x(2)\rangle/s^2 &= \langle[\cos(2k_Fx+\alpha)](1)[\cos(2k_Fx+\alpha)](2)\rangle\\ &= \cos(2k_Fx)\left(\frac{\xi_0}{\sqrt{(\tau v'_\alpha)^2+x^2}}\right)^{K'_\alpha/2}.\end{aligned} \tag{94}$$

Due to $SO(2)$-symmetry in the x–y-plane, this is the same as the $\langle S^yS^y\rangle$ correlation function. The transverse spin rotation correlation function is

$$\langle S^x(1)S^y(2)\rangle/s^2 = \sin(2k_Fx)\left(\frac{\xi_0}{\sqrt{(\tau v'_\alpha)^2+x^2}}\right)^{K'_\alpha/2}. \tag{95}$$

Equation (95) reveals the spin rotation (helical configuration) in the EP case, see figure 8. Contrary to the EA case, the Fourier transform of the dynamical in-plane spin susceptibility

$$\langle S^+(1)S^-(2)\rangle/s^2 = 2(\langle S^x(1)S^x(2)\rangle - \mathrm{i}\langle S^xS^y\rangle)/s^2 = \exp(-\mathrm{i}2k_Fx)\left(\frac{\xi_0}{\sqrt{(\tau v'_\alpha)^2+x^2}}\right)^{K'_\alpha/2} \tag{96}$$

has a peak only at $2k_F$. The longitudinal spin correlator $\langle S^zS^z\rangle$ is zero in our accuracy (at fixed $\theta = 0$, $\alpha_\parallel = 0$).

6.3. Order parameter

We have shown that the low energy spin excitations of the EA case are planar spin oscillations, whereas in the EP case the spins form a helix, see figure 8.

The transverse spin correlation function $\langle S^x(1)S^y(2)\rangle$, which reflects rotations of the spins, is zero in the non-helical phase (EA), but nonvanishing in the helical one (EP). Thus we suggest to use it as an order parameter. In analogy with antiferromagnetic ordering [41], we define the two-point order parameter

$$\mathcal{A}_c = \epsilon_{abc}\langle S^a(1)S^b(1+\xi_0)\rangle, \tag{97}$$

which is non-vanishing only in the helical phase, where there is a low-energy helical mode propagating within the dense chain of the magnetic impurities.

7. Conclusion

Low-energy properties of an anisotropic KC away from half-filling are governed either by the Kondo screening or by the RKKY interaction generated by the backscattering of electrons on the spins. The latter process becomes dominant when the concentration of the spins is sufficiently large and when the repulsive electron–electron interactions are sufficiently strong. Then the RKKY interaction opens a gap in the quasiparticle spectrum, equation (24), which further suppresses the Kondo screening. Depending on the anisotropy of the exchange interaction, the backscattering processes may either lead to a formation of the CDWs and the SDWs (EA anisotropy), equation (28), or generate the helical low energy modes (EP anisotropy), equation (41). The appearence of such modes is related to spontaneous breking of the $\mathbb{Z}_2$(helical)-symmetry. We have shown that the order parameter characterizing the corresponding quantum phase transition is the average of the vector product of neighboring spins $\mathcal{A}_c = \epsilon_{abc}\langle S^a(1)S^b(1+\xi_0)\rangle$. The helical nature of the modes is also manifest in the asymmetry between the $+2k_F$ and $-2k_F$ peaks in the in-plane spin susceptibility $\langle S^+S^-\rangle$, equation (96). The ideal charge transport supported by the gapless helical modes is robust: it remains ballistic even if a weak random potential of static impurities is present. This protection requires the spin the $U(1)$ symmetry and exists up to the parametrically large scale, see equation (71). We have shown that short-range electron–electron interactions mix the two helical sectors, but cannot gap out any low-energy modes, such that for weak interactions the qualitative description in terms of the helical modes remains valid.

Even though the helical modes may be reminiscent of the edge modes of topological insulators, we emphasize that, in our case, they are generated by the many-body interactions in one spacial dimension. Experimentally, the helical modes could be detected in samples exhibiting one-dimensional structure with spin impurities. As we have discussed in Introduction, promising candidates are ladder-type Fe-selenides, where almost completely filled bands of electrons might serve as spin impurities [21], or single-wall carbon nanotubes functionalized by magnetic ions [18]. Since the advent of the cleaved edge overgrowth method [42], quantum wires on the edge of GaAs heterostructures are also viable candidates.

Usually, one cannot control the anisotropy of real materials. Therefore, one needs an experimental evidence that the charge transport in a given system with the dense array of the Kondo impurities is supported by modes with a broken helical symmetry. The cleanest signature could be provided by the local spin susceptibility (equations (89) and (96)), which clearly provides a smoking gun signature for the helical order. The local spin susceptibility may be experimentally accessible through nitrogen-vacancy based STM measurements if the Kondo array is made as a one-dimensional wire [43].

Another experimental signature of the helical phase is frequency-resolved charge transport. We remind the readers that in our model the charge is carried either by the collective mode α (EA), or by the collective mode α and the helical fermion (EP) with the velocity of the α-excitations being always small (equations (29) and (40)). If a sufficiently clean sample of a finite size is adiabatically connected to leads, its dc conductance remains ideal, $2e^2/h$ [44]. However, the frequency resolved conductance is expected to show a substantial decrease at $\omega_c \sim 1/t_{\rm Th}^{(\alpha)}$; where $t_{\rm Th}^{(\alpha)} \sim L/v_\alpha$ is the Thouless time associated with the mode α. Since the α-modes are very slow ω_c is small. For frequencies larger than ω_c, the slow collective modes cannot contribute and the conductance drops either to zero (EA) or to e^2/h (EP). The latter jump would confirm that the system is in the helical phase which is robust against localization effects.

A similar transition could also be detected at $\omega = 0$ in the temperature dependence of the conductance. We expect that at finite temperature domains of different helicity develop. At temperatures above the energy of a domain-wall ($T > E_{\rm domain\ wall}$) the quasiparticles do not contribute to the dc transport any longer and a crossover of the conductance from $2e^2/h$ to e^2/h is expected with increasing T. Hence, the T-dependence of the conductance at very small temperatures (possibly less than 5 mK reached in [45]) should be studied.

In order to check that the reduction of the conductance is related to the presence of the localized spins, one may repeating the measurements on samples where the magnetic atoms are not present. If the spin-spin

interaction is important the presence or absence of the additional localized spins will have a strong influence on the conductance. Finally, we have shown that the helical transport is partially protected from localization effects. This means that the conductance will not change even if the sample length becomes longer than the mean-free path of the material.

The theory of the frequency and temperature dependent conductance of the KC requires further theoretical work.

Acknowledgments

AMT acknowledges the hospitality of Ludwig Maximilians University where part of this work was done. AMT was supported by the US Department of Energy (DOE), Division of Materials Science, under Contract No. DE-AC02-98CH10886. OMYe acknowledges support from the DFG through SFB TR-12, and the Cluster of Excellence, Nanosystems Initiative Munich. DHS is supported through by the DFG through the Excellence Cluster Nanosystems Initiative Munich, SFB/TR 12 and SFB 631. We are grateful to Vladimir Yudson and Igor Yurkevich for useful discussions.

Appendix A. Derivation of the low-energy Lagrangian

In this section we give a short derivation of the form of the electron-spin interactions in terms of the fast and slow angular variables ($\alpha_\parallel$, $\alpha_\perp$, θ, and ψ). Thus, consider the interaction term

$$H_{\rm int} = \sum_m J_a\, \hat{c}_m^\dagger\, \hat{\sigma}^a \hat{S}^a(m)\, \hat{c}_m. \tag{A1}$$

Using the representation of the fermions in terms of left- and rightmovers, equation (9), this term splits into forward and backward scattering contributions

$$H_{\rm int} = H_{\rm forward} + H_{\rm backward}, \tag{A2}$$

$$H_{\rm forward} = \sum_m J_a^{\rm f}\, \hat{R}_m^\dagger\, \hat{\sigma}^a \hat{S}^a(m)\, \hat{R}_m + \sum_m J_a^{\rm f}\, \hat{L}_m^\dagger\, \hat{\sigma}^a \hat{S}^a(m)\, \hat{L}_m, \tag{A3}$$

$$H_{\rm backward} = +\sum_m J_a^{\rm b} e^{2ik_{\rm F}x}\, \hat{R}_m^\dagger\, \hat{\sigma}^a \hat{S}^a(m)\, \hat{L}_m + \sum_m J_a^{\rm b} e^{-2ik_{\rm F}x}\, \hat{L}_m^\dagger\, \hat{\sigma}^a \hat{S}^a(m)\, \hat{R}_m, \tag{A4}$$

where the superscript f (b) denotes forward (backward) scattering contributions. Using the low-energy spin $S_{\rm LE} \| \boldsymbol{e}_3'$ and taking the dense impurity limit, we obtain

$$\begin{aligned}\mathcal{L}_{\rm int}^{\rm (bs)} = s\rho_{\rm s} e^{2ik_{\rm F}x} R^\dagger \Big\{ \tfrac{J_\perp^{\rm b}}{2} [&+ e^{i\nu\psi}(-\cos\alpha_\parallel \cos\alpha_\perp \cos\theta - i\cos\alpha_\parallel \sin\alpha_\perp + \sin\alpha_\parallel \sin\theta)\hat{\sigma}^- \\ &+ e^{-i\psi}(-\cos\alpha_\parallel \cos\alpha_\perp \cos\theta + i\cos\alpha_\parallel \sin\alpha_\perp + \sin\alpha_\parallel \sin\theta)\hat{\sigma}^+] \\ &+ J_z^{\rm b}\hat{\sigma}_z(\sin\alpha_\parallel \cos\theta + \cos\alpha_\parallel \cos\alpha_\perp \sin\theta)\Big\} L + {\rm h.c.}.\end{aligned} \tag{A5}$$

This expresses the back-scattering part of the electron-spin interaction in terms of the angular variables and the fermions. To obtain the low-energy part, we first shift $\alpha_\perp \to \alpha(x) + 2k_{\rm F}x$. Then, neglecting all quickly oscillating terms ($\sim e^{4ik_{\rm F}x}$), equation (A5) reduces to

$$\begin{aligned}\mathcal{L}_{\rm int}^{\rm (sl)\,(bs)} = \frac{s\cos(\alpha_\parallel)\rho_{\rm s}}{2} R^\dagger \left\{ J_\perp \left[e^{i\psi} \sin^2\left(\frac{\theta}{2}\right)\hat{\sigma}^- - e^{-i\psi}\cos^2\left(\frac{\theta}{2}\right)\hat{\sigma}^+ \right] + J_z \sin(\theta)\hat{\sigma}^z \right\} L e^{-i\alpha} \\ + {\rm h.c.}; \quad \tilde{s} \equiv s\cos(\alpha_\parallel).\end{aligned} \tag{A6}$$

The forward-scattering part of the action is obtained by following the same procedure with $H_{\rm forward}$:

$$\mathcal{L}_{\rm int}^{\rm (sl)\,(fs)} = \frac{s\sin(\alpha_\parallel)\rho_{\rm s}}{2} R^\dagger \{ J_\perp^{\rm f} \sin\theta [e^{i\psi}\sigma^- + e^{-i\psi}\sigma^+] + 2J_z^{\rm f}\cos\theta\sigma^z \} R + (R \to L). \tag{A7}$$

Appendix B. Bosonization and the RG equations

Here we briefly remind readers of the bosonization identity used throughout, and the derivation of the RG equations. We only derive one RG equation explicitely, but the other RG equations may be obtained by the same procedure.

The bosonization formula is

$$\Psi_{r\sigma} = \frac{1}{\sqrt{2\pi\alpha}} U_\sigma \mathrm{e}^{-\mathrm{i}rk_\mathrm{F}x} \mathrm{e}^{-\frac{1}{\sqrt{2}}\mathrm{i}[r\Phi_\mathrm{c}-\Theta_\mathrm{c}+\sigma(r\Phi_\mathrm{s}-\Theta_\mathrm{s})]}, \tag{B1}$$

where Φ_c (Φ_s) and Θ_c (Θ_s) are dual fields belonging to the charge (spin) density wave, r distinguishes right- and left-moving and σ is the spin. The Klein factors U_σ are real coordinate independent fermionic operators obeying the anticommutation relations $\{U_\sigma, U_{\sigma'}\} = \delta_{\sigma,\sigma'}$.

After bosonization equation (B1), the electron-spin interaction contains the terms

$$\begin{aligned}
\mathcal{L}_z^\mathrm{f} &:= J_z^\mathrm{f} S_z (R^\dagger \sigma_z R + L^\dagger \sigma_z L) = -\sqrt{2} S_z \frac{J_z^\mathrm{f}}{\pi} \partial_x \Phi_\mathrm{s}, \\
\mathcal{L}_-^\mathrm{f} &:= J_\perp^\mathrm{f} S_- (R^\dagger \sigma_+ R + L^\dagger \sigma_+ L) = S_- \frac{J_\perp^\mathrm{f}}{\pi\xi_0} \exp(-\sqrt{2}\mathrm{i}\Theta_\mathrm{s})(\exp(\sqrt{2}\mathrm{i}\Phi_\mathrm{s}) + \exp(-\sqrt{2}\mathrm{i}\Phi_\mathrm{s})), \\
\mathcal{L}_+^\mathrm{f} &:= J_\perp^\mathrm{f} S_+ (R^\dagger \sigma_- R + L^\dagger \sigma_- L) = S_+ \frac{J_\perp^\mathrm{f}}{\pi\xi_0} \exp(\sqrt{2}\mathrm{i}\Theta_\mathrm{s})(\exp(-\sqrt{2}\mathrm{i}\Phi_\mathrm{s}) + \exp(\sqrt{2}\mathrm{i}\Phi_\mathrm{s})), \\
\mathcal{L}_z^\mathrm{b} &:= J_z^\mathrm{b} S_z (R^\dagger \sigma_z L + L^\dagger \sigma_z R) = S_z \frac{J_z^\mathrm{f}}{2\pi\xi_0} \exp(-2\mathrm{i}k_\mathrm{F}x) \exp(\sqrt{2}\mathrm{i}\Phi_\mathrm{c})(\exp(\sqrt{2}\mathrm{i}\Phi_\mathrm{s}) - \exp(-\sqrt{2}\mathrm{i}\Phi_\mathrm{s})) + \mathrm{h.c.}, \\
\mathcal{L}_-^\mathrm{b} &:= J_\perp^\mathrm{b} (S_- R^\dagger \sigma_+ L + S_+ L^\dagger \sigma_- R) = S_- \frac{J_\perp^\mathrm{f}}{\pi\xi_0} \exp(-2\mathrm{i}k_\mathrm{F}x) \exp(\sqrt{2}\mathrm{i}(\Phi_\mathrm{c} - \Theta_\mathrm{s})) + \mathrm{h.c.}, \\
\mathcal{L}_+^\mathrm{b} &:= J_\perp^\mathrm{b} (S_+ R^\dagger \sigma_- L + S_- L^\dagger \sigma_+ R) = S_+ \frac{J_\perp^\mathrm{f}}{\pi\xi_0} \exp(-2\mathrm{i}k_\mathrm{F}x) \exp(\sqrt{2}\mathrm{i}(\Phi_\mathrm{c} + \Theta_\mathrm{s})) + \mathrm{h.c.}.
\end{aligned} \tag{B2}$$

The flow of the coupling constants is obtained by integrating out high energy modes. To do so, one must split Φ_α, Θ_α and S_β into fast (superscript $>$) and slow (superscript $<$) modes:

$$\Phi_\alpha = \Phi_\alpha^< + \Phi_\alpha^>, \quad \Theta_\alpha = \Theta_\alpha^< + \Theta_\alpha^>, \quad S_\beta = S_\beta^< + S_\beta^>. \tag{B3}$$

The measure of the path integral splits into fast and slow modes as well. We then perform the integral over the fast modes in a perturbative series in J and reexponentiate the result. The first order in J leads to the one-loop RG equations. As in the bosonization treatment of the Kondo impurity, we will treat the spins as constant during the RG flow. Thus, we need to compute

$$\int \mathcal{D}\{\Phi, \Theta\} \exp\left(-S_\mathrm{LL}[\Phi, \Theta] - \int \mathrm{d}\tau \mathrm{d}x J_a S_a f_a(\Phi, \Theta)\right), \tag{B4}$$

where S_LL is the Luttinger liquid action for Φ and Θ and f_a is a function which can be read off from (B2). Note that there is space–time UV cutoff ξ_0 (or equivalently an energy–momentum cutoff Λ). Let us consider as an example the term proportional to J_z^b:

$$\begin{aligned}
&\int \mathcal{D}\{\Phi^>, \Theta^>\} \exp(-S_\mathrm{LL}[\Phi^>, \Theta^>]) \int \mathrm{d}\tau \mathrm{d}x J_z^\mathrm{b} S_z^< f_z^\mathrm{b}(\Phi^> + \Phi^<, \Theta^> + \Theta^<) \\
&= \int \mathrm{d}\tau \mathrm{d}x J_z^\mathrm{b} S_z^< \int \mathcal{D}\{\Phi^>, \Theta^>\} \exp(-S_\mathrm{LL}[\Phi^>, \Theta^>]) \frac{1}{2\pi\xi_0} \exp(-2\mathrm{i}k_\mathrm{F}x) \exp(\sqrt{2}\mathrm{i}(\Phi_\mathrm{c}^> + \Phi_\mathrm{c}^<)) \\
&\quad \times (\exp(\sqrt{2}\mathrm{i}(\Phi_\mathrm{s}^> + \Phi_\mathrm{s}^<)) - \exp(-\sqrt{2}\mathrm{i}(\Phi_\mathrm{s}^> + \Phi_\mathrm{s}^<))) + \mathrm{h.c.}
\end{aligned} \tag{B5}$$

The components $\Phi^>$ ($\Theta^>$) and $\Phi^<$ ($\Theta^<$) are of high and low energy, such that the energy of $\Phi^>$ ($\Theta^>$) lies in the interval $[\Lambda', \Lambda]$. Using the equalities $\langle \mathrm{e}^{\sqrt{2}\mathrm{i}\Phi_\mathrm{s}^>} \rangle_> = (\Lambda'/\Lambda)^{K_\mathrm{s}/2}$ and $\langle \mathrm{e}^{\sqrt{2}\mathrm{i}\Theta_\mathrm{s}^>} \rangle_> = (\Lambda'/\Lambda)^{1/(2K_\mathrm{s})}$, we can perform the average over fast modes. This yields

$$\begin{aligned}
&\int \mathcal{D}\{\Phi^>, \Theta^>\} \exp(-S_\mathrm{LL}[\Phi^>, \Theta^>]) \int \mathrm{d}\tau \mathrm{d}x J_z^\mathrm{b} S_z^< f_z^\mathrm{b}(\Phi^> + \Phi^<, \Theta^> + \Theta^<) \\
&= \int \mathrm{d}\tau \mathrm{d}x J_z^\mathrm{b} S_z^< \left(\frac{\Lambda'}{\Lambda}\right)^{\frac{1}{2}(K_\mathrm{s}+K_\mathrm{c})} f_z^\mathrm{b}(\Phi^<, \Theta^<).
\end{aligned} \tag{B6}$$

Since the cutoff was changed from Λ' to Λ, we need to rescale x and τ to recover the original expression. Reexponentiating (B6) yields

$$J_z^\mathrm{b}(\Lambda') = J_z^\mathrm{b}(\Lambda) \left(\frac{\Lambda'}{\Lambda}\right)^{\frac{1}{2}(K_\mathrm{s}+K_\mathrm{c})-2}. \tag{B7}$$

The RG equation is obtained expressing equation (B7) as a differential equation in the parametrization $\Lambda' = \Lambda \mathrm{e}^{-l-dl}$, where dl is an infinitesimal number:

$$\partial_l J_z^{\rm b} = \left[\tfrac{1}{2}(K_{\rm s}+K_{\rm c})-2\right]J_z^{\rm b}. \tag{B8}$$

Appendix C. The shift of the angles in the EA case

We present a short, alternative derivation of the action after the shift eliminiating the angles α and ψ from the interaction vertices, equation (22). This proof is based on abelian bosonization. Upon bosonization, equation (B1), the free part of the Lagrangian are a spin and charge Tomonaga–Luttinger liquid:

$$\mathcal{L} = \mathcal{L}_{\rm TL,dual}[\Phi_{\rm c},\Theta_{\rm c}] + \mathcal{L}_{\rm TL,dual}[\Phi_{\rm s},\Theta_{\rm s}], \tag{C1}$$

with

$$\mathcal{L}_{\rm TL,dual}[\Phi_a,\Theta_a] = -\frac{\rm i}{\pi}\partial_x\Theta_a\partial_\tau\Phi_a + \frac{1}{2\pi}\left(uK(\partial_x\Theta_a)^2 + \frac{u}{K}(\partial_x\Phi_a)^2\right). \tag{C2}$$

We use a description in terms of fields Φ and their duals Θ. The shift equation (19) is in bosonic language

$$\Phi_{\rm c} \to \Phi_{\rm c} + \alpha/\sqrt{2},\ \Theta_{\rm s} \to \Theta_{\rm s} - \psi/\sqrt{2}. \tag{C3}$$

Performing this shift also in the Tomonaga–Luttinger liquid equation (C1), we obtain the new terms of the form

$$\mathcal{L}_{\rm mixing} \sim -{\rm i}\partial_\tau\alpha\partial_x\Theta_{\rm c} - \partial_x\alpha\partial_x\Phi_{\rm c} - {\rm i}\partial_\tau\psi\partial_x\Phi_x - \partial_x\psi\partial_x\Theta_{\rm s}. \tag{C4}$$

and terms of the type

$$\mathcal{L}_{\rm TL,dual}[\alpha/\sqrt{2},\Theta_{\rm c}] + \mathcal{L}_{\rm TL,dual}[\Phi_{\rm s},\psi/\sqrt{2}]. \tag{C5}$$

Since after bosonization spatial derivatives of $\Phi_{\rm c/s}$ ($\Theta_{\rm c/s}$) correspond to the charge/spin density (current), equation (C4) contains precisely the terms of equation (21), and may be neglected by the same arguments. After averaging over the dual fields $\Theta_{\rm c}$ and $\Phi_{\rm s}$, equation (C5) is the same as the Tomonaga–Luttinger anomaly equation (20). We thus have obtained the same expression as in the main text, without explicitely using the Tomonaga–Luttinger anomaly.

Appendix D. Accounting for interactions

In this section we show how to obtain equation (47). We start from the bosonized Lagrangian of interacting electrons

$$\mathcal{L} = -\frac{\rm i}{\pi}\partial_x\Theta_{\rm c}\partial_\tau\Phi_{\rm c} + \frac{1}{2\pi}\left(u_{\rm c}K_{\rm c}(\partial_x\Theta_{\rm c})^2 + \frac{u_{\rm c}}{K_{\rm c}}(\partial_x\Phi_{\rm c})^2\right) - \frac{\rm i}{\pi}\partial_x\Theta_{\rm s}\partial_\tau\Phi_{\rm s} + \frac{1}{2\pi}\left(u_{\rm s}K_{\rm s}(\partial_x\Theta_{\rm s})^2 + \frac{u_{\rm s}}{K_{\rm s}}(\partial_x\Phi_{\rm s})^2\right). \tag{D1}$$

In order to rewrite equation (D1) in terms of helical fields, we define

$$\Phi_{h_1} = \tfrac{1}{\sqrt{2}}(\Phi_{\rm c}-\Theta_{\rm s}),\quad \Theta_{h_1} = \tfrac{1}{\sqrt{2}}(\Theta_{\rm c}-\Phi_{\rm s}), \tag{D2a}$$

$$\Phi_{h_2} = \tfrac{1}{\sqrt{2}}(\Phi_{\rm c}+\Theta_{\rm s}),\quad \Theta_{h_2} = \tfrac{1}{\sqrt{2}}(\Theta_{\rm c}+\Phi_{\rm s}). \tag{D2b}$$

This choice stems from the identities

$$\begin{aligned}\rho_\downarrow^R &= \frac{\sqrt{2}}{\pi}\partial_x(\Theta_{\rm c}-\Phi_{\rm c}-(\Theta_{\rm s}-\Phi_{\rm s})),\\ \rho_\uparrow^L &= \frac{\sqrt{2}}{\pi}\partial_x(-\Theta_{\rm c}-\Phi_{\rm c}-\Theta_{\rm s}-\Phi_{\rm s}).\end{aligned} \tag{D3}$$

If there are no particles of one specific helical sector (e.g. $R_\downarrow$ and $L_\uparrow$), then both of these densities should vanish. This is guaranteed if there are no fluctuations in Φ_{h2} and Θ_{h2}. Thus, the fields Φ_{h2} and Θ_{h2} correspond to the helical sector containing $R_\downarrow$ and $L_\uparrow$.

Inserting equation (D2*a*) into equation (D1), we obtain

$$\begin{aligned}2\mathcal{L} =& -\frac{\rm i}{\pi}\partial_x(\Theta_{h_1}+\Theta_{h_2})\partial_\tau(\Phi_{h_1}+\Phi_{h_2}) + \frac{1}{2\pi}\left(u_{\rm c}K_{\rm c}(\partial_x(\Theta_{h_1}+\Theta_{h_2}))^2 + \frac{u_{\rm c}}{K_{\rm c}}(\partial_x(\Phi_{h_1}+\Phi_{h_2}))^2\right)\\ &-\frac{\rm i}{\pi}\partial_x(-\Phi_{h_1}+\Phi_{h_2})\partial_\tau(-\Theta_{h_1}+\Theta_{h_2}) + \frac{1}{2\pi}\left(u_{\rm s}K_{\rm s}(\partial_x(-\Phi_{h_1}+\Phi_{h_2}))^2 + \frac{u_{\rm s}}{K_{\rm s}}(\partial_x(-\Theta_{h_1}+\Theta_{h_2}))^2\right)\end{aligned} \tag{D4}$$

$$= -2\tfrac{\mathrm{i}}{\pi}\partial_x(\Theta_{h_1})\partial_\tau(\Phi_{h_1}) + \tfrac{1}{2\pi}\left(\left(u_\mathrm{c}K_\mathrm{c} + \tfrac{u_\mathrm{s}}{K_\mathrm{s}}\right)(\partial_x\Theta_{h_1})^2 + \left(\tfrac{u_\mathrm{c}}{K_\mathrm{c}} + u_\mathrm{s}K_\mathrm{s}\right)(\partial_x\Phi_{h_1})^2\right)$$
$$- 2\tfrac{\mathrm{i}}{\pi}\partial_x(\Theta_{h_2})\partial_\tau(\Phi_{h_2}) + \tfrac{1}{2\pi}\left(\left(u_\mathrm{c}K_\mathrm{c} + \tfrac{u_\mathrm{s}}{K_\mathrm{s}}\right)(\partial_x\Theta_{h_2})^2 + \left(\tfrac{u_\mathrm{c}}{K_\mathrm{c}} + u_\mathrm{s}K_\mathrm{s}\right)(\partial_x\Phi_{h_2})^2\right)$$
$$+ \tfrac{1}{2\pi}\left(2\left(u_\mathrm{c}K_\mathrm{c} - \tfrac{u_\mathrm{s}}{K_\mathrm{s}}\right)\partial_x\Theta_{h_2}\partial_x\Theta_{h_1} + 2\left(\tfrac{u_\mathrm{c}}{K_\mathrm{c}} - u_\mathrm{s}K_\mathrm{s}\right)\partial_x\Phi_{h_2}\partial_x\Phi_{h_1}\right). \tag{D5}$$

The shift equation (35), which keeps the second helical sector invariant, corresponds to $\Phi_{h_1} \to \Phi_{h_1} + \alpha/2$. After neglecting couplings between gapless modes and derivatives of the first helical sector, we find in addition to the free part $\mathcal{L}_\mathrm{TL}$ of α

$$\mathcal{L} = -\tfrac{\mathrm{i}}{\pi}\partial_x\Theta_{h_1}\partial_\tau\Phi_{h_1} + \tfrac{1}{4\pi}\left(\left(u_\mathrm{c}K_\mathrm{c} + \tfrac{u_\mathrm{s}}{K_\mathrm{s}}\right)(\partial_x\Theta_{h_1})^2 + \left(\tfrac{u_\mathrm{c}}{K_\mathrm{c}} + u_\mathrm{s}K_\mathrm{s}\right)(\partial_x\Phi_{h_1})^2\right)$$
$$- \tfrac{\mathrm{i}}{\pi}\partial_x\Theta_{h_2}\partial_\tau\Phi_{h_2} + \tfrac{1}{4\pi}\left(\left(u_\mathrm{c}K_\mathrm{c} + \tfrac{u_\mathrm{s}}{K_\mathrm{s}}\right)(\partial_x\Theta_{h_2})^2 + \left(\tfrac{u_\mathrm{c}}{K_\mathrm{c}} + u_\mathrm{s}K_\mathrm{s}\right)(\partial_x\Phi_{h_2})^2\right)$$
$$+ \tfrac{1}{2\pi}\left(\tfrac{u_\mathrm{c}}{K_\mathrm{c}} - u_\mathrm{s}K_\mathrm{s}\right)\partial_x\Phi_{h_2}\partial_x\alpha. \tag{D6}$$

Introducing

$$\tilde{K} = \sqrt{\frac{u_\mathrm{c}K_\mathrm{c} + \frac{u_\mathrm{s}}{K_\mathrm{s}}}{\frac{u_\mathrm{c}}{K_\mathrm{c}} + u_\mathrm{s}K_\mathrm{s}}}, \quad \tilde{u} = \frac{1}{4}\sqrt{u_\mathrm{c}^2 + u_\mathrm{s}^2 + u_\mathrm{c}u_\mathrm{s}K_\mathrm{c}K_\mathrm{s} + \frac{u_\mathrm{c}u_\mathrm{s}}{K_\mathrm{c}K_\mathrm{s}}}, \tag{D7}$$

equation (D6) may be written as

$$\mathcal{L} = -\tfrac{\mathrm{i}}{\pi}\partial_x\Theta_{h_1}\partial_\tau\Phi_{h_1} + \tfrac{1}{2\pi}\left(\tilde{u}\tilde{K}(\partial_x\Theta_{h_1})^2 + \tilde{u}\tfrac{1}{\tilde{K}}(\partial_x\Phi_{h_1})^2\right)$$
$$- \tfrac{\mathrm{i}}{\pi}\partial_x\Theta_{h_2}\partial_\tau\Phi_{h_2} + \tfrac{1}{2\pi}\left(\tilde{u}\tilde{K}(\partial_x\Theta_{h_2})^2 + \tilde{u}\tfrac{1}{\tilde{K}}(\partial_x\Phi_{h_2})^2\right)$$
$$+ \tfrac{1}{2\pi}\left(\tfrac{u_\mathrm{c}}{K_\mathrm{c}} - u_\mathrm{s}K_\mathrm{s}\right)\partial_x\Phi_{h_2}\partial_x\alpha. \tag{D8}$$

Appendix E. Non-Gaussianities in the effective disorder

In this appendix, we demonstrate that the higher moments of the effective disorder g_eff distribution function in the alternative approach to disorder are of higher order in $\frac{\mathcal{D}}{v_\mathrm{F}m} \ll 1$. Thus, in our accuracy, we may safely neglect the non-Gaussianities of the effective disorder.

We have assumed that the distribution of the $2k_\mathrm{F}$ Fourier components of the original disorder potential is Gaussian, however the distribution of $g_\mathrm{eff}(x)$ is not Gaussian. To investigate the effect of the non-Gaussianity of the distribution function of the effective disorder g_eff, we consider its moments. The first moment is zero:

$$\langle g_\mathrm{eff}(x)\rangle_\mathrm{dis} \sim \left\langle \frac{1}{v_\mathrm{F}}\int \mathrm{d}y g(x + y/2)g(x - y/2)\mathrm{e}^{-m|y|/v_\mathrm{F}}\right\rangle_\mathrm{dis} = 0, \tag{E1}$$

because g is distributed according to the GUE. The second moment is given by

$$\langle g_\mathrm{eff}(x)g_\mathrm{eff}(x')\rangle_\mathrm{dis} \sim \left\langle \frac{1}{v_\mathrm{F}^2}\int \mathrm{d}y\mathrm{d}\tilde{y} g(x + y/2)g(x - y/2)g(x' + \tilde{y}/2)g(x' - \tilde{y}/2)\mathrm{e}^{-m(|y|+|\tilde{y}|)/v_\mathrm{F}}\right\rangle_\mathrm{dis} = 0, \tag{E2}$$

and

$$\begin{aligned}\langle g_\mathrm{eff}(x)g^*_\mathrm{eff}(x')\rangle_\mathrm{dis} &\sim \tfrac{1}{v_\mathrm{F}^2}\left\langle \int \mathrm{d}y\mathrm{d}\tilde{y}\ g(x + y/2)g(x - y/2)g^*(x' + \tilde{y}/2)g^*(x' - \tilde{y}/2)\mathrm{e}^{-m(|y|+|\tilde{y}|)/v_\mathrm{F}}\right\rangle_\mathrm{dis}\\ &\sim \frac{\mathcal{D}^2}{v_\mathrm{F}^2}\int \mathrm{d}y\mathrm{d}\tilde{y}(\delta(x + y/2 - x' + \tilde{y}/2)\delta(x - y/2 - x' - \tilde{y}/2)\\ &\qquad + \delta(x + y/2 - x' - \tilde{y}/2)\delta(x - y/2 - x' + \tilde{y}/2))\mathrm{e}^{-m(|y|+|\tilde{y}|)/v_\mathrm{F}}\\ &\sim \tfrac{\mathcal{D}^2}{v_\mathrm{F}m}\delta(x - x').\end{aligned} \tag{E3}$$

Higher moments contain additional contractions, reflecting the non-Gaussianity of the distribution of g_eff. As an example, consider the fourth moment

$$\langle g_{\rm eff}(x)g_{\rm eff}(y)g^*_{\rm eff}(z)g^*_{\rm eff}(w)\rangle_{\rm dis} \sim \frac{1}{\nu_{\rm F}^4}\Big\langle \int {\rm d}x'{\rm d}y'{\rm d}z'{\rm d}w'\; g(x+x'/2)g(x-x'/2)g(y+y'/2)g(y-y'/2) \times g^*(z+z'/2)g^*(z-z'/2)g^*(w+w'/2)g^*(w-w'/2) \times {\rm e}^{-m(|x'|+|y'|+|z'|+|w'|)/\nu_{\rm F}}\Big\rangle_{\rm dis}. \tag{E4}$$

There are two distinct kinds of contractions: Gaussian ones (contracting e.g. $\langle g(x+x'/2)g^*(z+z'/2)\rangle$, $\langle g(x-x'/2)g^*(z-z'/2)\rangle$, $\langle g(y+y'/2)g^*(w+w'/2)\rangle$, and $\langle g(y-y'/2)g^*(w-w'/2)\rangle$) and non-Gaussian ones, e.g. contracting $\langle g(x-x'/2)g^*(z-z'/2)\rangle$, $\langle g(x+x'/2)g^*(w+w'/2)\rangle$, $\langle g(y+y'/2)g^*(z+z'/2)\rangle$, and $\langle g(y-y'/2)g^*(w-w'/2)\rangle$. The latter yields:

$$\begin{aligned}\langle g_{\rm eff}(x)g_{\rm eff}(y)g^*_{\rm eff}(z)g^*_{\rm eff}(w)\rangle_{\rm dis} &\supset \frac{\mathcal{D}^4}{\nu_{\rm F}^4}\int {\rm d}x'{\rm d}y'{\rm d}z'{\rm d}w'\delta(x-x'/2-z+z'/2)\delta(x+x'/2-w-w'/2) \\ &\quad\times\delta(y+y'/2-z-z'/2)\delta(y-y'/2-w+w'/2) \\ &\quad\times{\rm e}^{-m(|x'|+|y'|+|z'|+|w'|)/\nu_{\rm F}} \\ &\sim \frac{\mathcal{D}^4}{\nu_{\rm F}^4}\int {\rm d}x'{\rm d}y'{\rm d}z'{\rm d}w'\delta(z'-y+x-y'/2-x'/2)\delta(w'-x \\ &\quad+y-y'/2-x'/2) \\ &\quad\times\delta(x'-2w+2z-y')\delta(z+w-x-y) \\ &\quad\times{\rm e}^{-m(|x'|+|y'|+|z'|+|w'|)/\nu_{\rm F}} \\ &\sim \frac{\mathcal{D}^4}{\nu_{\rm F}^4}\delta(z+w-x-y)\int {\rm d}y'{\rm e}^{-m(|2w-2z+y'|+|y'|+|y'-2z+2y|+|2w-2y+y'|)/\nu_{\rm F}}.\end{aligned} \tag{E5}$$

In addition to the phase space factor of $\nu_{\rm F}/m$, we obtain an exponential suppression of lengths $(w-z)$ etc larger than $\nu_{\rm F}/m$. The leading order for large distances may be extracted by formally taking the limit $m\to\infty$. The exponential may then be approximated by a δ-function: $\delta(x)=\lim_{m\to\infty}(m/\nu_{\rm F})\exp(-m|x|/\nu_{\rm F})$. Note that in the case of multiple terms in the exponent some of them might be spurious, i.e. $\exp(-m(|x|+|x|)/\nu_{\rm F})\sim(\nu_{\rm F}/m)\delta(x)$. Taking this into account the large-distance limit of equation (E5) leads to

$$\langle g_{\rm eff}(x)g_{\rm eff}(y)g^*_{\rm eff}(z)g^*_{\rm eff}(w)\rangle_{\rm dis} \sim \frac{\mathcal{D}^4}{\nu_{\rm F}^4}\delta(z+w-x-y)\frac{\nu_{\rm F}^3}{m^3}\delta(z-w)\delta(y-w). \tag{E6}$$

Higher moments are suppressed in a similar fashion. Thus, we have proven that the non-Gaussian contributions are supressed by at least the factor $\frac{\mathcal{D}^2}{(\nu_{\rm F}m)^2}$.

References

[1] Gulácsi M 2004 *Adv. Phys.* **53** 769
[2] Braunecker B, Simon P and Loss D 2009 *Phys. Rev.* B **80** 165119
[3] Klinovaja J, Stano P, Yazdani A and Loss D 2013 *Phys. Rev. Lett.* **111** 186805
[4] Gulacsi M 2004 *Adv. Phys.* **53** 769
[5] Maciejko J 2012 *Phys. Rev.* B **85** 245108
[6] Tsunetsugu H, Sigrist M and Ueda K 1997 *Rev. Mod. Phys.* **69** 809
[7] Zachar O, Kivelson S A and Emery V J 1996 *Phys. Rev. Lett.* **77** 1342
[8] Honner G and Gulacsi M 1997 *Phys. Rev. Lett.* **78** 2180
[9] Novais E, Miranda E, Castro Neto A H and Cabrera G G 2002a *Phys. Rev.* B **66** 174409
[10] Novais E, Miranda E, Castro Neto A H and Cabrera G G 2002b *Phys. Rev. Lett.* **88** 217201
[11] Shibata N, Ishii C and Ueda K 1995 *Phys. Rev.* B **51** 3626
[12] White S R and Affleck I 1996 *Phys. Rev.* B **54** 9862
[13] Juozapavicius A, McCulloch I P, Gulacsi M and Rosengren A 2002 *Phil. Mag.* B **82** 1211
[14] Pfeiffer L, Strmer H, Baldwin K, West K, Goi A, Pinczuk A, Ashoori R, Dignam M and Wegscheider W 1993 *J. Cryst. Growth* **127** 849
[15] Wegscheider W, Kang W, Pfeiffer L, West K, Stormer H and Baldwin K 1994 *Solid-State Electron.* **37** 547
[16] Tarucha S, Honda T and Saku T 1995 *Solid State Commun.* **94** 413
[17] Maslov D L 1995 *Phys. Rev.* B **52** R14368
[18] Simon F, Kramberger C, Pfeiffer R, Kuzmany H, Zólyomi V, Kürti J, Singer P M and Alloul H 2005 *Phys. Rev. Lett.* **95** 017401
[19] Rmmeli M H *et al* 2007 *J. Phys. Chem.* C **111** 4094
[20] Churchill H O H, Bestwick A J, Harlow J W, Kuemmeth F, Marcos D, Stwertka C H, Watson S K and Marcus C M 2009 *Nat. Phys.* **5** 321
[21] Rincón J, Moreo A, Alvarez G and Dagotto E 2014 *Phys. Rev. Lett.* **112** 106405
[22] Caron J M, Neilson J R, Miller D C, Llobet A and McQueen T M 2011 *Phys. Rev.* B **84** 180409
[23] Luo Q *et al* 2013 *Phys. Rev.* B **87** 024404
[24] Nambu Y *et al* 2012 *Phys. Rev.* B **85** 064413
[25] Tsvelik A M and Yevtushenko O M 2015 *Phys. Rev. Lett.* **115** 216402
[26] Moore J E and Balents L 2007 *Phys. Rev.* B **75** 121306(R)
[27] Maciejko J, Liu C, Oreg Y, Qi X L, Wu C and Zhang S C 2009 *Phys. Rev. Lett.* **102** 256803

[28] Roy R 2009 *Phys. Rev.* B **79** 195321
[29] Xu C and Moore J E 2006 *Phys. Rev.* B **73** 045322
[30] Franz M and Molenkamp L 2013 *Topological Insulators* (Amsterdam: Elsevier)
[31] Kurita M, Yamaji Y and Imada M 2015 arXiv:1511.02532
[32] Kawakami T and Hu X 2016 *J. Phys. Soc. Jpn.* **85** 013701
[33] Altshuler B L, Aleiner I L and Yudson V I 2013 *Phys. Rev. Lett.* **111** 086401
[34] Yevtushenko O M, Wugalter A, Yudson V I and Altshuler B L 2015 *EPL* **112** 57003
[35] Tsvelik A M 2003 *Quantum Field Theory in Condensed Matter Physics* (Cambridge: Cambridge University Press)
[36] Schrieffer J R 1967 *J. Appl. Phys.* **38** 1143
[37] Grishin A, Yurkevich I V and Lerner I V 2004 *Phys. Rev.* B **69** 165108
[38] Gogolin A O, Nersesyan A A and Tsvelik A M 1998 *Bosonization and Strongly Correlated Systems* (Cambridge: Cambridge University Press)
[39] Giamarchi T 2004 *Quantum Physics in One Dimension* (Oxford: Clarendon, Oxford University Press)
[40] Giamarchi T and Schulz H J 1988 *Phys. Rev.* B **37** 325
[41] Fradkin E 2013 *Field Theories of Condensed Matter Physics* (Cambridge: Cambridge University Press)
[42] Pfeiffer L, Yacoby A, Stormer H, Baldwin K, Hasen J, Pinczuk A, Wegscheider W and West K 1997 *Microelectron. J.* **28** 817
[43] Stano P, Klinovaja J, Yacoby A and Loss D 2013 *Phys. Rev.* B **88** 045441
[44] Maslov D L and Stone M 1995 *Phys. Rev.* B **52** R5539(R)
[45] Scheller C P, Liu T-M, Barak G, Yacoby A, Pfeiffer L N, West K W and Zumbühl D M 2014 *Phys. Rev. Lett.* **112** 066801